Nano Today 27 (2019) 11–27

Contents lists available at ScienceDirect

Nano Today

journal homepage: www.elsevier.com/locate/nanotoday

Toward large-scale water treatment using nanomaterials

Wei Zhao [a], I-Wei Chen [b,**], Fuqiang Huang [a,c,*]

[a] State Key Laboratory of High Performance Ceramics and Superfine Microstructure, Shanghai Institute of Ceramics, Chinese Academy of Sciences, Shanghai, 200050, PR China
[b] Department of Materials Science and Engineering, University of Pennsylvania, Philadelphia, PA19104, USA
[c] Beijing National Laboratory for Molecular Sciences and State Key Laboratory of Rare Earth Materials Chemistry and Applications, College of Chemistry and Molecular Engineering, Peking University, Beijing, 100871, PR China

ARTICLE INFO

Article history:
Received 26 November 2018
Received in revised form 9 April 2019
Accepted 21 May 2019
Available online 5 June 2019

Keywords:
Water Treatment
Adsorption
Advanced Oxidation Processes
Photocatalysis
Three-dimensional Graphene
Black Titania
Field Application

ABSTRACT

Water pollution worldwide has already endangered health and environment. At places of rapid population growth and urbanization, traditional technologies for wastewater treatment and polluted water reclamation are approaching their limits. Nanomaterials of small particle sizes, huge specific surface areas and abundant reactive sites are ideal for adsorbing pollutants, but semiconducting nanoparticles that can harness sunlight to catalyze advanced oxidation processes are especially effective for eliminating refractory water contaminants. This paper reviews the guiding principles of nanomaterial adsorption and photocatalysis for advanced water treatment, and calls attention to low-cost, high-performance nanomaterials that are well positioned for large-scale water treatment. Black titania (BT) capable of full-spectrum solar photon absorption and three-dimensional graphene (3DG) with an unparalleled combination of electrical conductivity, mechanical strength/flexibility and surface activity and functionality are especially promising. Hybrids of BT and 3DG have been successfully field-tested for large-area remediation of contaminated water in its natural setting, and the lessons learned will lead to further advances in this technology, including ones that integrate wastewater treatment with energy conversion and storage.

Contents

Abbreviations: 3DG, three dimensional graphene; NS, nanosheet; AC, activated carbon; NW, nanowire; AOP, advanced oxidation processes; OH, hydroxyl radicals; BET, burnauer-emmett-teller; PC, photocatalysis; BOD, biochemical oxygen demand; PCE, perchloroethylene; BT, black titania; PEC, photoelectrocatalysis; CBM, conduction band minimum; PF, packing factor; CE, counter electrode; PFC, photocatalytic fuel cell; CNT, carbon nanotube; PVC, photovoltaic cell; COD, chemical oxygen demand; RGO, reduced graphene oxide; CVD, chemical vapor deposition; ROS, reactive oxygen species; EC, electrocatalysis; SCE, saturated calomel electrode; FTO, fluorine doped tin oxide; SG, spongy graphene; GO, graphene oxide; TCE, trichloroethylene; MB, methylene blue; TiO_2,, titanium dioxide; MO, methyl orange; TGH, titania-graphene hydrogel; NHE, normal hydrogen electrode; TOC, total organic carbon; NP, nanoparticle; UV, ultraviolet; NR, nanorod; VBM, valence band maximum.

* Corresponding author at: State Key Laboratory of High Performance Ceramics and Superfine Microstructure, Shanghai Institute of Ceramics, Chinese Academy of Sciences, Shanghai, 200050, PR China.
** Corresponding author.
E-mail addresses: iweichen@seas.upenn.edu (I.-W. Chen), huangfq@mail.sic.ac.cn (F. Huang).

https://doi.org/10.1016/j.nantod.2019.05.003
1748-0132/

Introduction

Water pollution caused by domestic, industrial, commercial and agricultural activities is a concern in both developed and developing worlds [1]. Water pollution is the leading cause of deaths and diseases in developing world, where 2.2 million people die each year because of unsanitary water that is consumed by 1 billion people everyday [2]. Even in the US, it is estimated that the national health system annually spends an additional 7 billion dollars to overcome the health problems caused by polluted water, and families without access to clean water and sanitation facilities incur another US$340 yearly cost each [3]. Because pollution increases with human activities, the problem may become more severe in the future, and as population and population density grow, water pollution will be compounded by water shortage. Indeed, if the current population trend and usage pattern continue, by 2025, four billion people will be living with severe water scarcity or shortage [4]. Therefore, there is an urgent need to develop effective and economic technology for water treatment, water reclamation and water reuse.

Wastewater is the most likely source of water pollution in most communities, and this has led to regulations for treating wastewater and setting the specifications for treated water before it can be reused, reclaimed or released. In addition to biological pollutants, wastewater often contains undesirable inorganic and organic chemicals shown in Table 1. The goal of the treatment is to completely remove such substance or to reduce it to below a certain level, such as the ones in the WHO guideline [5], to ensure human health and environmental safety. Municipal wastewater treatment is undertaken by either public utility or private for-profit business. (In special circumstances, wastewater treatment can be a profitable endeavor; for example, when Au^+ and Ag^+ are recovered from gold/silver plant liquids, slurries, and effluents that contain $Au(CN)_2$ and $Ag(CN)_2$.) However, standard wastewater treatment technologies—adsorption, chemical or biological treatment, and membrane-based separation or filtration—are beginning to be pushed to their limits by the rapid population growth and large-scale industrialization and urbanization in many populous developing countries. This has led to the call for new technologies with higher efficiencies and lower costs, many of them based on nanomaterials [6].

Ref: WHO, Guidelines for drinking-water quality (fourth edition), WHO Library Cataloguing-in-Publication Data, 2017.

Overview of water treatment technology and the need for nanomaterials

In a municipal setting, water treatment is a systematic project of multiple steps (Fig. 1) [7]. Primary treatment holds the wastewater in a quiescent tank resulting in the settlement of heavy suspensions to the bottom, and lighter ones, such as oil and grease, to the surface. It may also include an additional step by adding inorganic or organic coagulants to the remaining liquid to cause flocculation of suspended particles that are subsequently removed by sedimentation and filtration. The remaining liquid usually contains less than half of the original particle content and approximately two-thirds of the dissolved and colloidal *organic* compounds measured by biochemical oxygen demand (BOD). Secondary treatment is designed to remove at least 85% BOD to a monthly averaged level of less than 30 mg/l and a like amount for suspended solids. This may be achieved by chemical or biochemical oxidation that converts organics into small inorganic molecules such as water, carbon dioxide, and salts, a process also referred to as mineralization. In some cases, favorable geological environments providing sand filtration may achieve the same outcome without mineralization. Tertiary treatment, often called advanced treatment, further removes biological nutrients (mainly nitrogen and phosphorus) and biologically toxic materials, and it also disinfects. This is achieved by adsorbing refractory pollutants using suitable adsorbents, such as in membrane separation. After this step, the treated water is nearly indistinguishable from water of natural origin, and it can be discharged to the receiving environment (sea, river, lake, waste lands, ground, etc.) Alternatively, tertiary treatment may involve advanced oxidation processes (AOPs), which are a set of chemical treatment procedures designed to remove organic and sometimes inorganic materials by oxidation through reaction with hydroxyl radicals (·OH), causing mineralization [8].

The above sequence is also embodied in typical unit operations of an industrial wastewater treatment plant: an oil-water separator, a clarifier for removing solids from wastewater, a roughing filter to reduce the BOD, a carbon filtration plant to remove toxic dissolved organic compounds, and an advanced electrodialysis reversal system with ion exchange membranes to further polish water quality. Agricultural wastewater treatment for continuous confined animal operations like milk and egg production may be performed by a similar set of unit operations. Wherever land is available, ponds, settling basins and facultative lagoons may be utilized to lower the operational costs.

It has been increasingly realized that nanomaterials may contribute to advanced water treatment technologies [9]. Nanomaterials are materials with a particle size of 100 nm or smaller. Compared with their bulk counterparts, nanomaterials having smaller sizes impart orders of magnitude higher specific surface area and surface reactive-sites. Many nanomaterials also feature tunable physical, chemical, and electronic properties that are not manifest in the bulk materials [10]. Although soft nanomaterials such as surfactants are commonly used to control coagulation and flocculation, the most critical new contributions the nanomaterials can make lie in filtration, adsorption and AOP. Carbonaceous nanomaterials (charcoal, activated carbon, and newer nanocarbon polymorphs such as carbon nanotube and graphene) have already found use in filtration and adsorption by virtue of their huge surface area and tailored pore sizes, which are important attributes for adsorption [11]. Meanwhile, various oxides (TiO_2, ZnO, Fe_2O_3, Fe_3O_4, WO_3, etc.) and metal (Fe, Ag) nanoparticles are highly effective for AOP because they generate, *in situ*, active hydroxyl radicals with the help of primary oxidants (ozone, hydrogen peroxide and oxygen), ultraviolet light or semiconductor photocatalysts, thereby achieving mineralization [8]. Using these nanoparticles, the concentration of contaminants can be reduced from the ppm level to the ppb level, hence significantly lowering BOD, chemical oxygen demand (COD) and total organic carbon (TOC). Indeed, it is

Table 1
Harmful chemicals in wastewater.

Sources	Inorganic	Guideline value (mg/L)	Organic	Guideline value (mg/L)
Naturally occurring	Arsenic	0.01	Microcystin-LR	0.001 (P)
	Barium	1.3		
	Boron	2.4		
	Chromium	0.05 (P)		
	Fluoride	1.5		
	Selenium	0.04 (P)		
	Uranium	0.03 (P)		
Industrial andhuman dwellings	Cadmium	0.003	Benzene	0.01
	Mercury	0.006	1,2-Dichlorobenzene	1 (C)
			1,4-Dichlorobenzene	0.3 (C)
			1,2-Dichloroethane	0.03
			1,2-Dichloroethene	0.05
			Dichloromethane	0.02
			1,4-Dioxane	0.05
			Edetic acid	0.6
			Ethylbenzene	0.3 (C)
			Nitrilotriacetic acid	0.2
			Styrene	0.02 (C)
			Tetrachloroethene	0.04
			Toluene	0.7 (C)
			Trichloroethene	0.02 (P)
			Xylenes	0.5 (C)
Agricultural activities	Nitrate	50	Alachlor	0.02 (A)
	nitrite	3	Aldicarb	0.01
			Chlorotoluron	0.03
			Chlorpyrifos	0.03
			1,2-Dichloropropane	0.04 (P)
			1,3-Dichloropropene	0.02 (A)
			Dichlorprop	0.1
			Hydroxyatrazine	0.2
			Mecoprop	0.01
			Trifluralin	0.02

(A) Substances that are carcinogenic; (C) concentrations at or below the health-based guideline value may still affect the appearance, taste or odor of water; (P) provisional guideline value because of uncertainties in the health database.

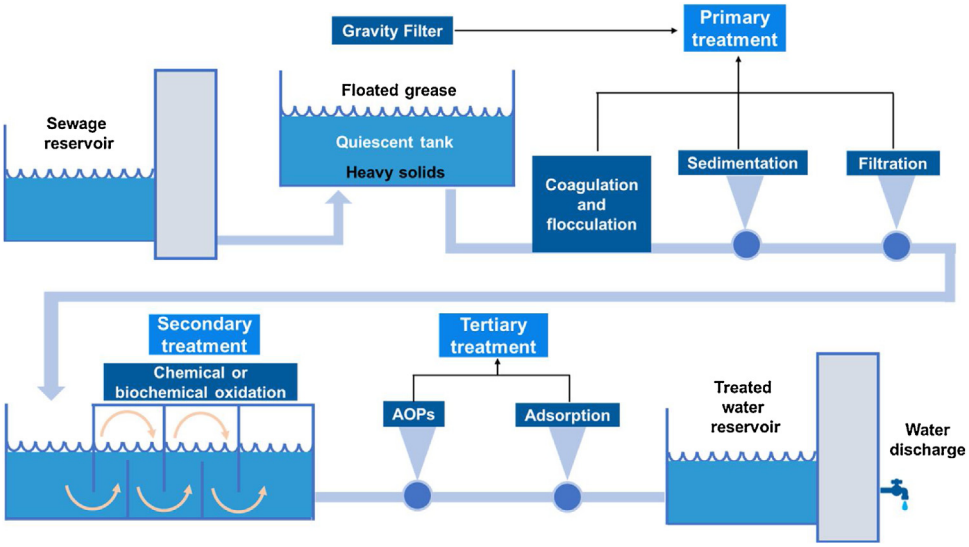

Fig. 1. Flow chart of multi-step wastewater treatment from primary to tertiary.

even possible to envision combining carbonaceous species and AOP-enabling nanoparticles to form material systems to realize synergistic effects, and to deploy them for one-time or short-term remediation of endangered water resources of ponds, lakes, rivers, wetlands, and grounds for which a permanent water treatment facility may not be necessary [12].

This paper will review the basic principles and advanced concepts of filtration, adsorption and AOP in connection to nanomaterials. Since strategic applications of nanomaterials in large-scale water treatment will critically depend on material availability and costs, those nanomaterials that have already made great strides in bulk synthesis, cost reduction and field demonstration at the pilot plant level are of special interest. These include three-dimensional graphene (3DG), black titania (BT) and 3DG/BT composites. The

paper will close with an outlook of future technologies that integrate wastewater treatment with energy production and storage.

Adsorption and filtration

Adsorption and filtration can facilitate separation of contaminants from the treated effluent. Membrane filtration via size-exclusion filters physically separates particles into different type of contaminants (suspended particles, bacteria, macromolecules, proteins, viruses, inorganic salts, etc.) and removes them: microfiltration for a mean pore size ultrafiltration for nanofiltration for and reverse osmosis for $\leq$ 1 nm) [13]. Adsorption by high-surface-area adsorbents in tertiary treatment removes heavy metal ions or refractory organic pollutants. The process is based on the principle that absorption lowers the energy of the interface, which may be a solid-solid, solid-liquid, solid-gas, liquid-liquid, or liquid-gas interface [14]. Conceptually, *adsorption* is limited to the interface and may be distinguished from *absorption*, which involves bulk material, although thermodynamically and empirically adsorption often extends to several atomic layers into the bulk. The adsorption process is usually classified into two: physical adsorption through weak van der Waals forces, hydrogen bonding, electrostatic attraction and π-π interactions, and chemical adsorption in which new chemical bonds form between the adsorbates and the adsorbents [15]. A typical binding energy of physical adsorption is about while that of chemical adsorption may reach 1 to 10 eV. Adsorption is usually illustrated through isotherms, which is the amount of adsorbate on the adsorbent measured as a function of gas pressure or liquid concentration at a certain temperature. Commonly used adsorption isotherms are named after Henry, Freundlich, Langmuir and Burnauer-Emmett-Teller (BET), referring to their respective models derived on different assumptions [16].

Since adsorption increases with the specific surface area, surface-abundant silicates and aluminosilicates such as sand, clay, silica gel and natural/man-made zeolite (many used as molecular sieves), as well as carbon materials such as charcoal and activated carbon (AC), are most common adsorbents [17]. Carbon materials are especially favored due to their very high specific surface area per unit mass and outstanding ability to withstand a broad range of chemical and physical conditions [11].

Carbon materials have been used to remove toxic pollutants in low concentrations in aqueous solutions since 1700 when it was first discovered that charcoal (the forerunner of widely used AC) can adsorb specific species in a gas mixture (1773) and colored solution (1786) [18]. Swedish chemist von Ostreijko invented commercial AC in two patents in 1900 and 1901 that described physical and chemical activation of normal carbonaceous materials [18]. Today's AC has a specific surface area between 500 and 3000 $m^2 g^1$ (thus somewhat higher than that of zeolite whose range is 500-1000 $m^2 g^1$). It has a rich pore structure consisting of micro-, meso- and macropores endowed with abundant surface functional groups. It is such high surface area and the excellent stability in aqueous solution that makes AC a popular choice as a most effective adsorbent in wastewater treatment and water filtration/purification processes [19].

Both charcoal and AC are three-dimensional materials comprising a three-dimensional sp^3-C network, although there is also an abundance of graphitic sp^2-C in these materials. An entirely new family of nanocarbon, however, has been discovered in recent years that are all made of sp^2-C, its simplest form being graphene, which arranges C atoms into a two-dimensional hexagonal network, and as such it can be regarded as a one-atom-thick graphite [20]. When this layer is wrapped into a closed shell that resembles a soccer ball in shape, it is called a fullerene, which may be regarded as a zero-dimensional allotrope of carbon. Likewise, it can be rolled into a tube, called a carbon nanotube (CNT), which is a one-dimensional allotrope [21,22]. To complete the list, CNT of various diameters and shell thickness can be connected, mostly tetrahedrally, into a three-dimensional, open-cell, ultralight foam, which is loosely referred to as 3DG [23]. Lastly, they can all be modified or doped to incorporate surface functional groups [24]. These new carbon nanomaterials have been investigated for wastewater treatment, because their van der Waals forces enable physical adsorption and they additionally benefit from physical and chemical adsorption when surface functional groups are present [11,25,26].

Since all forms of carbon described above can obtain a porous structure, it is common to classify them into different types by pore size [27]. Microporous carbon has pores of less than 2 nm, mesoporous carbon and macroporous carbon >50 nm. Pores in ordered carbon are ordered because they are created by some templating process via a sacrificial template of an ordered mesoscopic network that is in turn derived from some surfactant-directed liquid-liquid phase separation process [28]. Similar mesoporous but disordered carbon is also easily obtained by pyrolysis of any number of suitable carbon-containing precursors of either a synthetic or a natural origin, such as plants or organisms [29,30]. In this respect, it should be mentioned that AC is too a disordered porous carbon with macropores, mesopores and micropores, and it is usually produced by carbonization of some carbonaceous natural materials such as coconut shell, with additional physical and/or chemical activation through oxidation in steam and/or impregnation of chemicals in the raw materials, before carbonization [31].

The presence of surface functional groups profoundly alters the characteristics of carbon, which is relevant to AOP. It introduces hydrophilic sites to an otherwise hydrophobic graphene surface. Adsorption of many molecular species from gas or liquid already occurs at the hydrophobic micro/mesoscopic pore surfaces of porous carbon, but surface functional groups provide much more potent sites for adsorption of ion species (either cationic or anionic) of metals and other organics/inorganics [25]. The chemical structures of such groups can be spectroscopically characterized and the overall pH and acidity/basicity of the carbons can be determined by titration. These characteristics are strongly correlated to the adsorption amount and adsorption enthalpy in an (ionic) species-dependent manner. In particular, there is direct evidence of charge transfer during adsorption; for example, the ratio of released protons to adsorbed cadmium ions on oxidized carbon of an AC is approximately 2, indicating cation exchange was involved in the process of adsorption, e.g., between H^+ (in the -COOH group) and Cd^{2+}. Such effect is powerful, for it results in dramatically enhanced Cd^{2+} adsorption even though the oxidation treatment (using HNO_3) actually lowers the specific surface area and pore volume somewhat. A further confirmation of this effect is provided by heat treatment above 300 °C, which decomposes the carboxylic acid group, and with it the enhanced Cd^{2+} adsorption is lost [32]. Just like oxidation can increase the surface acidity, nitridation and sulfuration of the AC surface can increase the surface basicity and polarity that strengthens specific interactions with (acidic) polar pollutants [31]. Since the agents of AOP are often supported by these carbon substrates, surface modification of the latter to enhance adsorption can create a "pre-concentration" effect of collecting pollutants locally, which makes subsequent AOP more efficient [12,33,34].

Advanced oxidation processes (AOP) and photocatalysis

Although a majority of contaminants in wastewater can be removed by standard primary and secondary treatments, some trace amount of non-degradable materials such as pharmaceutical residues are hard to eliminate. The limitations of conventional approaches provoked the development of more effective tech-

niques such as AOPs, which rely on highly reactive ·OH to oxidize organic (and sometimes inorganic as well) pollutants into water, carbon dioxide and salts [8]. Metallic nanoparticles such as Fe, Al and Ag can serve this purpose by providing direct oxidation [35]. This is not new. For example, developed in 1890s, Fenton's reagent is a solution of hydrogen peroxide with ferrous iron catalyst that is used to oxidize contaminants in wastewaters: it can destroy toxic organic compounds such as trichloroethylene (TCE) and tetrachloroethylene (perchloroethylene, PCE) [36]. In an aqueous environment, the reaction proceeds by

$$Fe^{2+}+H_2O_2= Fe^{3+}+\cdot OH + OH^-$$

$$Fe^{3+}+H_2O_2= Fe^{2+}+HO_2\cdot + H^+$$

with the net effect being a disproportionation of hydrogen peroxide. But Fe and Al can also act alone in an aqueous environment to generate hydrogen peroxide by various reactions such as

$$Fe + O_2+2H^+= Fe^{2+}+H_2O_2$$

$$Fe + H_2O_2+2H^+= Fe^{2+}+2H_2O$$

$$Fe^{2+}+H_2O_2= Fe^{3+}+\cdot OH + OH^-$$

and

$$Al = Al^{3+}+3e^-$$

$$O_2+H^++e^-= HO_2\cdot$$

$$HO_2\cdot = H_2O_2+O_2$$

$$Al + 3H_2O_2= Al^{3+}+3\cdot OH + 3OH^-$$

Therefore, metallic nanoparticles such as Fe, Al and other metal such as Ag can provide direct oxidation for AOP as well [37]. These reactions are irreversible, however, so fresh nanoparticles must be supplied for AOP to continue, which can be costly. Nevertheless, Ag nanoparticles and Ag^+ ions have been used for since ancient times, and it is now known that Ag or Ag^+ introduced into bacterial cells can also induce a high degree of oxidation-initiated structural and morphological changes that lead to cell death. So, despite its high cost, Ag is still used in critical applications [38].

A potentially cost-effective AOP agent is an oxide or chalcogenide semiconductor nanoparticle that undergoes heterogeneous photocatalysis [39,40]. The best example is titanium dioxide (TiO_2) [41]. The positive holes of TiO_2 have a strong oxidative potential that oxidizes water to create ·OH, and they can also oxidize oxygen or organic materials directly. Since the band gap of TiO_2, ~3 eV, falls into the UV range, these functions can be UV activated. Already widely used as pigment, TiO_2's ability to generate ·OH adds to its appeal in products of paints, cements, windows and tiles by imparting sterilizing, deodorizing and anti-fouling properties.

The photocatalytic properties of TiO_2 to generate ·OH were discovered by Fujishima:

$$TiO_2+h\nu \rightarrow TiO_2(h^++e^-)$$

$$TiO_2(h^+) + H_2O \rightarrow TiO_2+\cdot OH + H^+$$

$$TiO_2(h^+) + OH^-\rightarrow TiO_2+\cdot OH$$

$$OH + organicpollutants \rightarrow CO_2+H_2O$$

$$TiO_2(e^-) + O_2\rightarrow TiO_2+\cdot O_2^-$$

$$O_2^-+2H_2O \rightarrow 2\cdot OH + 2OH^-$$

$$O_2^-+2OH^-\rightarrow 2\cdot OH + O_2$$

$$OH + organicpollutants \rightarrow CO_2+H_2O$$

In this mechanism, known as the Honda-Fujishima effect, TiO_2 acts like a catalyst by providing photo-activated holes—it itself is not consumed unless photo bleaching occurs, and it generates no other byproduct than H_2O and CO_2. Importantly, too, the above effect requires no additional substance other than sunlight and natural oxygen, so it can occur under ambient conditions with a high turnover rate for repeated operation. Therefore, the process is potentially cost effective for detoxification or remediation of wastewater [42].

Other than TiO_2, a large number of photoactive semiconductors have also been explored as photocatalysts [43,44]. They include various metal oxides (ZnO, Fe_2O_3, Fe_3O_4, WO_3, Bi_2WO_6, Ag_3PO_4, etc.), chalcogenides (CdS, In_2S_3, MoS_2, ZnSe, etc.), and other types of compounds (C_3N_4, AgCl, BiOCl, etc.) For redox reactions in aqueous solutions, it is convenient to refer to the position of band edge shown in Fig. 2a, which indicates the vacuum level and the band gap in relation to the H_2/H^+ level (0 eV if measured against a normal hydrogen electrode or NHE) and the O_2/H_2O level (1.23 eV). Redox potentials of reactive oxygen species (ROS) relevant to water remediation, including $\cdot O_2^-$, H_2O_2 and ·OH, are also plotted in the figure. Oxide semiconductors are capable of generating ·OH because their valence band (VB, primarily composed of O 2*p* orbitals) typically lies above the $\cdot OH/H_2O$ level [45]. But TiO_2 is unique in that the electrons in its conduction band (CB) can be transferred to dissolved oxygen molecules to generate $\cdot O_2^-$, which can be further reduced to H_2O_2 and ·OH. This is unlike the case of ZnO, Fe_2O_3 and WO_3 for which the process does not work efficiently because their CB is lower. To utilize the full spectrum of solar energy, however, a band gap of is ideal, so there is a need to tailor the band structure as well other aspects of semiconductor carriers and defects to achieve efficient generation and utilization of electron-hole pairs and electron- or hole-initiated redox cascades [46]. More on them will be described in the next section.

Not only for its special band-structure levels but also in practical terms, TiO_2 has the unique potential to be deployed for wastewater treatment or water remediation. Being one of the most mass-produced inorganic nonmetal products, it already enjoys commercial success as a (low-purity) pigment/filler and a (high-purity) source-powder for fabricating electronic ceramics. But it is also notable for its thermodynamic stability. According to the Pourbaix diagram of the metal/H_2O system, most oxides are only stable for a limited pH range (WO_3: pH ZnO: pH Fe_2O_3: pH, but TiO_2 is stable from pH 2 to pH 13 [47], which is an important advantage for large-scale wastewater treatment and water remediation that may receive water of a broad and often uncontrolled chemistry.

To simplify recovery from the treated effluent, practical applications require nanoparticulate photocatalysts to be fixed on a support [48,49]. While the support is sometimes considered inert, there is ample evidence that it can also strongly influence the overall photocatalytic activity of nanoparticle catalysts. This is because different support can cause different amount of catalyst, and/or different amount of target organic/inorganic molecules for catalysis, to be absorbed, or it is simply because of different photocatalytic activity. The latter may be due to different light absorption by the support and/or different physical/chemical interactions between the catalyst and the support. Mechanistically, the physical interface between a catalyst and the support is pivotal as it affects stereochemistry and the energy bias/barrier for charge transfer and subsequent redox processes. Another factor is the surface func-

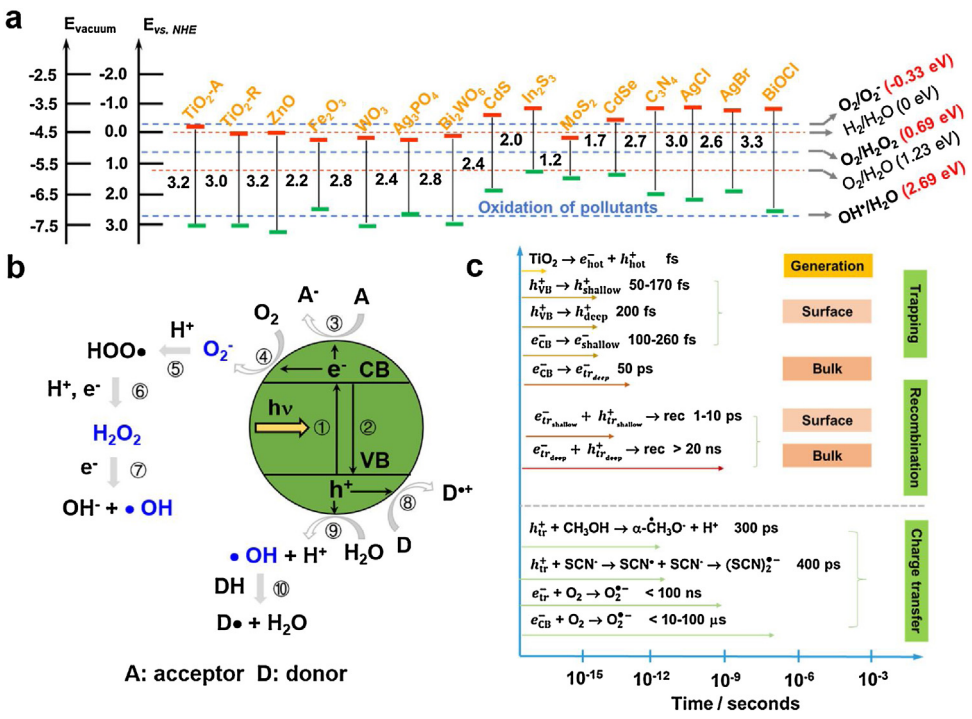

Fig. 2. (a) Band edges of common semiconductor photocatalysts versus redox potentials of hydrogen evolution reaction, oxygen evolution reaction and reactions of several reactive oxygen species relevant to wastewater treatment. (b) Schematic illustration of photocatalytic reaction occurring in and about TiO_2. 1. Bandgap excitation and electron-hole pairs generation, 2. electron–hole recombination, 3. electron capture by electron acceptor, 4. electron transfer to dissolved oxygen molecules, 5. formation of hydroxyperoxyl radical, 6. generation of hydrogen peroxide, 7. formation of hydroxyl radical, 8. hole transfer to electron donor, 9. hole transfer to surface hydroxyl group to generate hydroxyl radical, and 10. hydroxyl radical-mediated degradation of organics (Reproduced with permission from Ref. [52], Copyright © 2013 Elsevier). (c) Time scales of photo-induced reactions in and about TiO_2 including carrier trapping, recombination and transfer (Reproduced with permission from Ref. [51], Copyright © 2014 American Physical Society).

tional groups and surface charge on the support or the catalyst, which can influence pre-concentration of adsorbed molecules as they intervene during molecule/support collision and adsorption. Obviously, the specific surface area of the catalyst is always important. Examples of TiO_2-nanocarbon (AC, nanotubes, graphene and graphene oxides) combinations or hybrids that combine the features of catalytic support, functional group tuning and synergistic effects will be described in the next section after a closer look at semiconductor photocatalysis and the design principle of engineering a nanomaterial photocatalyst.

Light absorption, band structures and electron transport

Photocatalysis—a closer look

Broadly speaking, there are three steps in semiconductor photocatalysis: (i) light absorption exciting electron-hole pairs across the band gap; (ii) separated electrons and holes migrating to the semiconductor surfaces; and (iii) electron or hole reacting with surface-adsorbed acceptor or donor species to complete the reactions (Fig. 2b) [50]. Provided there is no charge buildup or poisoning, these steps can be repeated indefinitely. Clearly, all three steps need to be optimized to attain the ideal efficiency: in (i), the more the full light spectrum can be absorbed, the more the electron-hole pairs are generated; in (ii), the more the electrons and holes can avoid mutual annihilation by recombination, the more they will migrate to the surfaces to be available for surface reactions; in (iii), surface reactions can be optimized by tailoring the energetics of reactive species, their preconcentration, pH, and the assistance of implanted surface functional groups. To guide successful optimization of the three steps, it is necessary to appreciate the very different time scales at which myriad photoinduced reactions occur, for example, as shown in Fig. 2c for TiO_2 [51]. On the fastest end, the band gap excitation creates electron-hole pairs in the femtosecond time scale. These pairs are subsequently trapped in shallow trap states (in or deep trap states (200 fs-50 ps). The electrons and holes in shallow trap states recombine with each other in about while those in deep trap states need more than 20 ns. The reduction of O_2 by trapped electrons to generate $\cdot O_2^-$ (in less than 100 ns) is much faster than the direct reduction by electrons in the CB μs). Lastly, in TiO_2, hole transfer is often faster than electron transfer, and among all the steps the interfacial transfer of photogenerated electrons is usually the slowest. Therefore, this last step is rate-limiting and need promotion the most in order to enhance the photocatalytic reaction overall [52]. Generally, the pollutants in direct contact with the catalyst surface can undergo photocatalytic degradation enabled by photogenerated electrons or holes. The charge transfer rate depends on the difference between the redox potential of ROS and the redox potential of specific pollutant [51]. After charge transfer, how the photocatalytic degradation proceeds further depends on the radiation intensity, nature and concentration of the photocatalysts and the pollutants, pH of the system, *etc*, as detailed in several reviews [41–43].

As already mentioned, TiO_2 is the most promising choice for practical applications in wastewater treatment and water remediation. There are three common polymorphs of TiO_2: anatase, rutile and brookite (Fig. 3) [53]. In addition, there are many other less common polymorphs such as monoclinic TiO_2 as well as intermediate phases that are defect-mediated with ordered oxygen vacancies and attendant lattice reconstruction. Yet none of these polymorphs is a particularly efficient photocatalyst because (a) their band gaps depending on polymorphs, Table 2) all fall into the ultraviolet (UV) region, which covers only 5% of the total solar energy, and (b) some polymorphs suffer from high electron-hole recombination

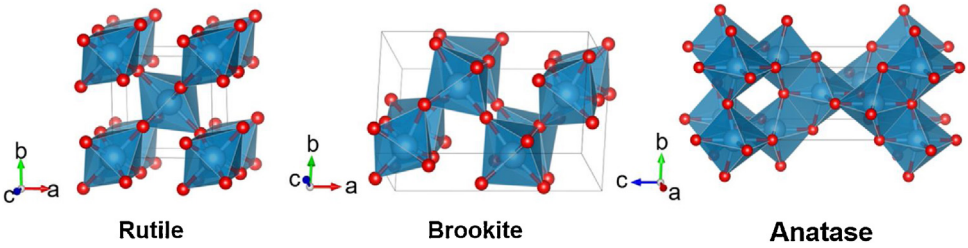

Fig. 3. Crystal structures of three polymorphs of TiO_2.

Table 2
Three polymorphs of TiO_2 and their structural parameters and packing factors (PFs).

Polymorphs	Space group	Unit cell and volume *a*, *b*, *c* (Å); β (deg); Volume (Å^3)	Band gap (eV)	PF	Photocatalytic activity
Anatase	$I4_1/amd$	$a = 3.79$, $c = 9.51$; $V = 136.3$	3.2	0.645	good
Rutile	$P4_2/mnm$	$a = 4.59$, $c = 2.96$; $V = 62.1$	3.0	0.705	Very poor
brookite	*Pbca*	$a = 9.18$, $b = 5.45$, $c = 5.15$; $\beta = 107.3$; $V = 258.9$	3.3	0.682	poor

rates leading to a low quantum efficiency [54]. This has motivated much research on modifying TiO_2 to extend its light absorption spectrum to the visible and near-infrared region and to promote efficient separation of electrons and holes [55].

The above consideration would seem irrelevant for nanocarbon since it mostly serves as an adsorbent or a preconcentration agent, and adsorption functions primarily rely on van der Waals interaction and surface functional groups. However, as we mentioned before, nanocarbon can also serve as a catalytic support for semiconductor photocatalysts and in this role it is sometimes capable of synergistic enhancement of photocatalytic activity. In such case its light absorption and electron conduction do become relevant. Indeed, nanocarbon/titania hybrids provide a fertile ground for developing high-performance AOP platforms. Therefore, maximized light absorption, optimized band structure and maximized electron transport quite generally hold the key to successful photocatalysts for wastewater treatment and water remediation technology.

Band structure modification for full-spectrum light absorption

Improved light absorption of TiO_2 can be realized by heteroatom doping (see schematic in Fig. 4a), organic dye sensitization, noble metal decoration and coupling with another narrow band-gap semiconductor [56]. Typically, introducing substitutional metal ions (Co, Ni, Mn, Fe, Cr, etc.) into the cation sublattice of TiO_2 leads to mid-gap states or reduces the band gap (between Ti-3*d* and O-2*p*), thus enhances visible-light absorption [57,58]. However, some *d*-block transition metal dopants have an adverse effect because they leave deeply localized *d*-gap-states that serve as recombination centers, and cation dopants with a closed shell electron configuration such as Zn provides no benefit. Anion dopants (N, S, C, F, I, P, etc.), on the other hand, are particularly effective because they cause *p*-orbital mixing, hence broadening, thus narrowing the band gap and increasing the activity [59]. But their overall effect is limited by the solubility, which is small because of their rather different sizes and electronic configurations from those of O^{2-}. Noble metal decoration creating local surface plasmon resonance may also enhance light harvesting [60], as does forming a heterojunction with a narrower band-gap semiconductor [61], but for cost considerations these strategies are not practical for large-scale applications.

A breakthrough in improving the light absorption efficiency of TiO_2 was made in 2011 by Chen et al., leading to various forms of black titania (BT) in subsequent years [62–73], In the initial work, hydrogenated nanoparticles with a crystalline (anatase) core and an amorphous shell, the latter with a disordered lattice, were discovered to exhibit enhanced light absorption efficiency and greatly improved photocatalytic activity. It was thought that the distorted lattice had distorted Ti-H and O-H bonds that provided mid-gap states and broadened the tail of valence band maximum (VBM), which allows the nanoparticle to extend the absorption edge to about 1.0 eV (~1200 nm) and realize a greatly reduced band gap of around 1.54 eV [62]. However, the process to obtain this BT (to be referred to as HP-TiO_2) requires a high-pressure () hydrogen treatment at 200 °C for five days, and its overall solar absorbance of about 30% (Table 3**)** left much to be desired.

Building on this discovery, our group used hydrogen plasma treatment at 500 °C for 8 h to generate a large amount of active H atoms that reached deeper inside the nanoparticle; the obtained BT (to be referred to as $TiO_{2-x}H_x$) features a solar absorbance of 83% (Table 3) [64]. Alternatively, reduction using metal Al reductant resulted in another BT (to be referred to as TiO_{2-x}) of 65% absorbance (Table 3), with improved visible and near-infrared absorption (Fig. 4b) [65]. Again, TiO_{2-x} contains a stoichiometric crystalline core (a mixture of anatase and rutile) and an oxygen-deficient amorphous shell, and its narrower band gap may be attributed to the broken symmetry and lattice destruction in the latter that broadens the tails of the VBM and the conduction band minimum (CBM), as schematically shown in Fig. 4c. Furthermore, the copious oxygen vacancies in the shell allow many oversized Ti^{3+} cations to form, which shifts the Fermi level towards the CBM. The black coloration partially originates from the electron transitions from Ti^{3+} $3d^1$ states to the unoccupied Ti 3*d* states, which goes beyond the earlier interpretation for H-doped amorphous shell in which oxygen vacancies and surface hydroxyl groups were thought to result in the black coloration by a process akin to the localized surface plasmon resonance seen after noble metal (Ag or Pt) decoration [64]. Lastly, Al reduction leaves a TiO_{2-x} host that has the unique capacity to incorporate a high concentration of anion dopants including N, S, and I (Fig. 4a), which is not possible in other TiO_2 or BT [74]. For example, shell compositions of 6.62 at.% N, 5.12 at.% S and 4.31 at.% I have all been achieved. Not surprisingly, such anion-doped BT further narrows the band gap and advances light harvesting (Fig. 4b). In particular, heavy N-doping boosts solar absorbance from 65% in TiO_{2-x} to 85% in N-doped TiO_{2-x} (Table 3). These various types of BT are generally capable of full-spectrum light absorption with an excellent performance in photocatalytic degradation of organic pollutants.

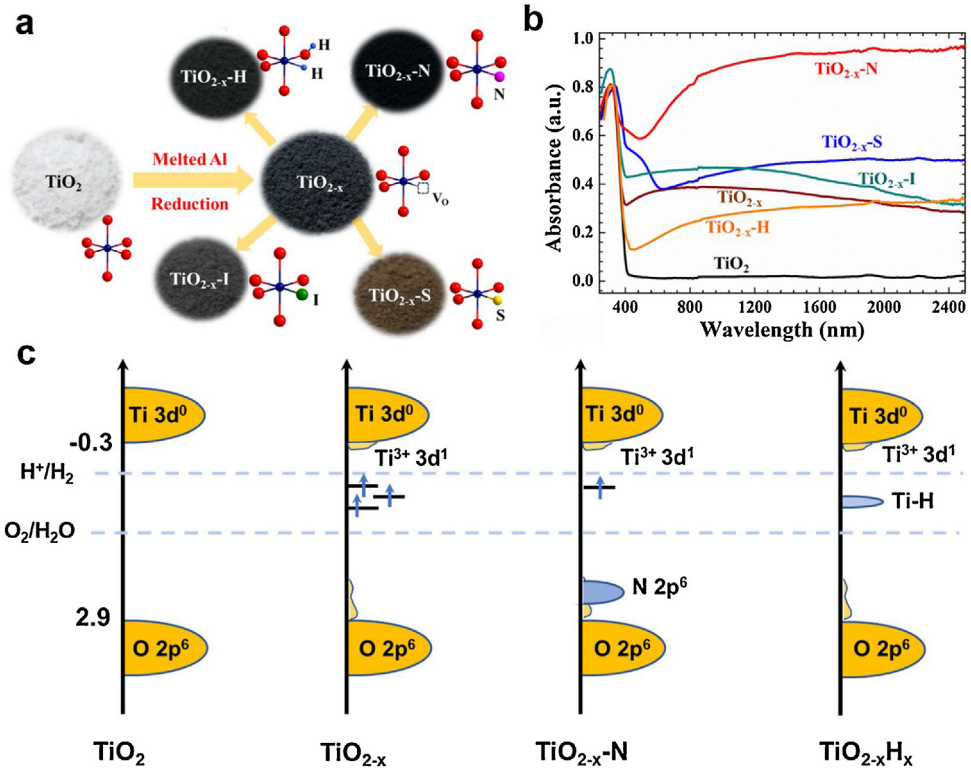

Fig. 4. (a) Schematic evolution from pristine TiO_2 to Al-reduced titania (TiO_{2-x}) and then to various nonmetal-doped TiO_{2-x} (TiO_{2-x}-nonmetal; nonmetal = H, N, S, I). (b) Absorption spectra of TiO_2 (P25, denoted by TiO_2), TiO_{2-x}, and various nonmetal-doped TiO_{2-x}. (c) Band structures of pristine TiO_2, Al reduced TiO_2 (TiO_{2-x}), N-doped TiO_{2-x} (TiO_{2-x}-N) and hydrogen plasma reduced TiO_2 ($TiO_{2-x}H_x$).

Table 3
Preparation methods, solar absorbance and photodecomposition time to reduce the concentration of MO below 5% of P25 vs. several BT produced in our group.

	Samples	Preparation methods	Solar absorbance (a.u.)				MO degradation time (min)	Ref
	Total (%)		UV (%)	Vis (%)	IR (%)			
	100		7	50	43			
White TiO_2	P25	Commercially available	5	5	0	0	20	[65]
Black titania (BT)	HP-TiO_2	High pressure hydrogen reduction	30	5	24	1	–	[62]
	TiO_{2-x}	Contactless Al reduction	65	5	32	28	12	[65]
	$TiO_{2-x}H_x$	Hydrogen plasma reduction	83	6	39	38	5	[64]
	TiO_{2-x}-N	Ammonia treatment of TiO_{2-x}	85	7	38	40	6	[74]

Charge transport and the packing-factor model

Photon-excited electron-hole pairs can reach very high densities when light absorption is efficient, yet most pairs are annihilated by recombination. Obviously, minimizing recombination and promoting effective charge separation by moving electrons and holes to different parts of the semiconductor are needed to greatly improve the efficiency of photocatalysis [75–77]. To achieve this, one well-known strategy is to minimize the concentration of recombination centers, C_{rec}. The other is to form heterostructures and p-n junctions as in solar cells. Regarding the former, nanomaterials have a distinct advantage in that the recombination distance being proportional to $C_{rec}^{1/2}$ only need to surpass the particle size, which is small in nanomaterials. So the task of lowering C_{rec} thus preventing recombination is less demanding in nanomaterials than in bulk materials. A lower C_{rec} can be achieved by a judicious selection of dopants and heat-treatment schedules, reducing the short dimension of a non-isometric nanoparticle, and providing suitable surface states that localize one carrier type but not the other [78]. To form heterostructures and p-n junctions, an approach commonly employed in solar cells, one needs to couple two semiconductors with either staggered band edges or p- and n-doping, which provides a bias for electron and hole separation [79]. This is difficult to achieve for nanoparticles by mass production.

In theory, a built-in internal electric field can also direct electrons and holes to migrate in opposite directions [80]. Such internal field does exist in polar materials, and in this connection ferroelectrics come immediately to mind. But the band gap of most ferroelectrics, typically greater than 3 eV, is too large for effective solar absorption, and the compositions of those ferroelectrics that do have a smaller band gap and exhibit somewhat robust photoelectric activities, such as $KBiFe_2O_5$ (band gap: 1.6 eV) and $[KNbO_3]_{0.9}[BaNi_{0.5}Nb_{0.5}O_{3-\delta}]_{0.1}$ (band gap: 1.4 eV), are probably not stable enough to withstand aqueous environments of a wide pH range that is demanded for wastewater treatment [81,82]. Interestingly, the three well-known polymorphs of TiO_2, tetragonal anatase, tetragonal rutile, and orthorhombic brookite, are themselves polar materials, so they should all support an internal field to some extent. These polymorphs share the same octahedral TiO_6 network: anatase comprises of edge-sharing octahedra, while rutile and brookite have both corner- and edge-sharing octahedral (Fig. 3) [53]. Not surprisingly, their band structures are not pronouncedly different. Yet anatase has the highest carrier mobility, the longest carrier diffusion length, and the most photocatalytic activity, in

sharp contrast with rutile that is the least active. As noted by our group, these distinctions can be understood by invoking the simple crystal-chemistry concept of packing factor (PF): compounds with a lower PF have a higher photoactivity [83–86]. Here, the PF of a compound $A_xB_yC_z$ is calculated by dividing the sum of spherical volumes of the constituents—V_A, V_B and V_C, obtained by using their respective Shannon radii—by the unit cell volume of the compound V_{cell}. That is,

$$PF = Z(xV_A + yV_B + zV_C)/V_{cell}$$

where Z is the number of formula units in one unit cell. A positive correlation between PF, lowest (0.645) for anatase and highest for rutile (0.705), and photoactivity, highest for anatase and lowest for rutile, then becomes evident (Table 2). (Brookite has an intermediate PF of 0.685 and an intermediate photoactivity.) The concept also led our group to predict BiO*X* (*X* = Cl, Br, I), which enjoys a low PF, should be an outstanding photocatalyst, which was indeed experimentally verified [87]. Physically, insulating compounds with a low PF are elastically soft. If their cations happen to have the d^0 configuration (like Ti^{4+}), then all their electrons must reside in the valence band manifold, and any lattice distortion that may accrue a large decrement in electronic energy will face little resistance as it only incurs a small penalty in elastic energy. Therefore, like first noted by Goodenough for d^0 ferroelectrics, a high-PF d^0 compound is prone to spontaneous coordinated lattice distortions that in turn induce an internal electric field beneficial for separating electrons and holes [88]. This, we believe, is the origin of enhanced photocatalytic activity of anatase.

Semiconductor-nanocarbon hybrids

As mentioned already, nanocarbon serving as a support offers its advantageous specific surface area and preconcentration effect to semiconductor photocatalysts. For such function, nanocarbon need not have good electron transport and light absorption, although it should not block light either. It turns out, however, that conductive nanocarbon does enhance the photocatalytic activity of semiconductors after all. Therefore, semiconductor-nanocarbon hybrids that are amenable to easy synthesis present an attractive advanced solution for AOP [89,90]. Before discussing this prospect, a brief word on nanocarbon conductivity is in order. While charcoal and AC are insulators, CNT has both the metallic conducting variety and the insulating variety depending on chirality, and graphene as well as 3DG are both metallic conductors. Meanwhile, graphene oxide (GO), which constitutes of various partially oxidized forms of graphene with certain ratios of C, O and H while still remaining two-dimensional and single-layer, is insulating because its C-sp^2 bonding network is severely disrupted [91]. But its reduced form, called reduced graphene oxide (RGO), is reasonably conducting [92]. Therefore, there is a continuum in electrical conductivity of graphene, RGO and GO, which happens to coincide with their continuous hydrophobic-to-hydrophilic transition.

All forms of carbon have proved to be a useful support for TiO_2 that enhances the photocatalytic activity [12]. With AC as support, commercially available TiO_2 nanoparticles, such as Degussa P25 (a mixture of anatase and rutile phase; average particle size of 25 nm), can avoid aggregation even at high loading. The AC/TiO_2 composites may be obtained by mechanical mixing, low temperature hydrolysis, sol-gel reaction, hydrothermal deposition, and chemical vapor deposition (CVD), and they all show enhanced photocatalytic water decontamination over P25 alone [93]. Nevertheless, AC is far from ideal because (i) the majority of its micropores are not accessible to P25, which usually occupies mesopores and macropores, (ii) inert AC has no chemical bonding with TiO_2, and (iii) insulating AC does not provide conducting pathways for electrons and holes. In contrast, conducting CNT with C-sp^2 bonding can hybridize with various TiO_2 nanostructures, including nanoparticles (NP), nanorods (NR), nanowires (NW) and nanosheets (NS), to form diverse nanocomposites [94,95]. Processed in benign solvents, hybrids of NP-TiO_2/CNT obtained through *in situ* nucleation and growth of NP-TiO_2 on single-walled CNT (400-900 $m^2\,g^1$) or multi-walled CNT (200-400 $m^2\,g^1$), some even on the inner surface of the tubes, display a higher photocatalytic activity than pristine, unsupported NP-TiO_2 [96]. This enhancement is attributed to a space charge region (electrically a double layer like a parallel plate capacitor) formed at the CNT/TiO_2 interface that promotes the transfer of photogenerated electrons, from the TiO_2's CBM to CNT, the latter providing an electron sink thus benefitting carrier separation. It was also found that CNT is itself a sensitizer and, once excited, can supply an electron to TiO_2's CBM. In the latter mechanism, a charge cycle is completed when the positively charged CNT captures an electron from TiO_2's VBM, effectively leaving another electron-hole pair in TiO_2 ready for catalytic reactions [97].

Combining BT with conductive carbon allotropes to form highly active hybrids for photocatalytic reaction has also been reported. These investigations used preparation methods such as hydrothermal synthesis, vacuum activation, laser ablation and UV-microwave treatments [98–101]. For example, Xing et al. developed a hydrothermal method to form composites of reduced TiO_2 NRs and boron-doped graphene from the co-reduction of GO and TiO_2 by $NaBH_4$ [101]. They reported improved visible-light photocatalytic activity on dyes and phenols, and the enhanced performance was ascribed to the synergistic effect between (a) Ti^{3+} as a self-dopant in TiO_2 to increase light harvesting and (b) boron doping to facilitate hole transfer and effective charge separation. Currently, the scientific investigation on BT/carbon composites is at an early stage so a full exploration of their potential in water treatment and other fields still awaits further studies [102]. However, in **Section 6.3**, we shall report our experience of using a BT/graphene construct for large-scale field applications in water treatment.

Turning to GO, Kamat and co-workers discovered that UV-activated TiO_2 deposition on ethanol-suspended GO can be used to form a RGO/TiO_2 hybrid (Fig. 5**a**) [103]. Hydrophilic GO used here has abundant carbonyl, hydroxyl and carboxyl functional groups, which provide affinity to TiO_2 and help disperse/process GO in polar solvents (Fig. 5b). After UV-irradiation, TiO_2 nanoparticles in size) were successfully deposited on RGO (Fig. 5c). It is also possible to achieve chemical bonding and GO reduction in a one-pot hydrothermal process involving P25; the end product is a P25/RGO hybrid with an enhanced adsorption capacity for organic dye, extended light absorption, and efficient charge separation. The giant π-π conjugation between methylene blue (MB, a commonly used target organic dye) and the aromatic graphene regions of RGO contributes to MB preconcentration, while RGO as a large aromatic-conjugated compound absorbs long-wavelength solar energy (Fig. 5d) [104]. Moreover, chemical bonding between P25 and RGO forming Ti-O-C bond causes a red shift of the TiO_2's absorption edge thus narrowing the band gap (Fig. 5**e**). The resultant hybrid finds a lower Fermi level in rGO relative to the CBM of TiO_2. So again, the RGO/TiO_2 interface under UV and visible light serves as an electron sink that helps carrier separation, enhances electron transport and reduces recombination, all leading to significantly improved photocatalytic degradation of MB than P25 alone (Fig. 5f).

With the increasing availability of 3DG, attention has recently turned to 3DG/TiO_2 hybrids [105]. In terms of wastewater treatment, their light-weight, stand-alone 3D structure offers considerable advantages in robust mechanical strength, high electron conductivity and excellent adsorption capacity for organic pollutants [106]. For example, a freeze-dried P25/3DG hybrid reported

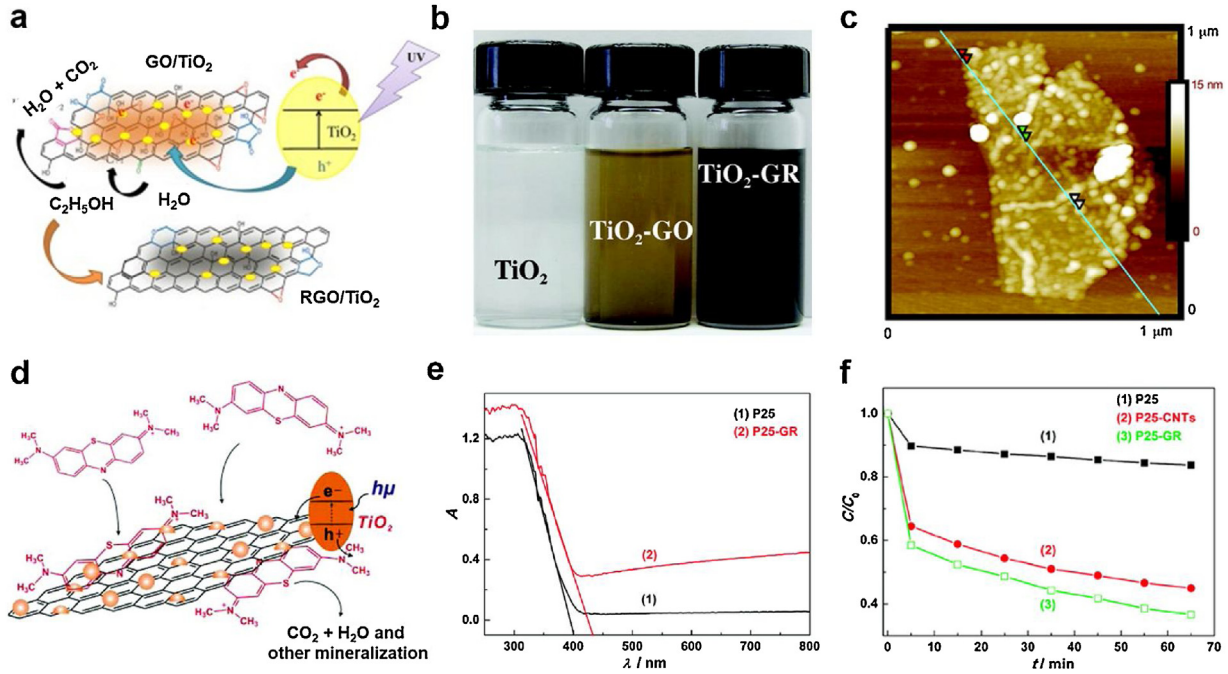

Fig. 5. (a) Formation of RGO/TiO_2 nanocomposites by simultaneous TiO_2 deposition and photocatalytic GO reduction under light illumination. (b) Photographs of TiO_2 colloidal suspension in ethanol (left), GO/TiO_2 mixture dispersed in ethanol (middle) and TiO_2-decorated RGO suspended in ethanol (right). (c) AFM image of TiO_2-decorated RGO (Reproduced with permission from Ref. [103], Copyright © 2008 American Physical Society). (d) Photodegradation mechanism of MB on P25-graphene nanocomposites. (e) Absorption spectra of P25-graphene nanocomposites and P25. (f) Photocatalytic degradation of methylene blue (MB) under visible light by (1) P25, (2) P25-CNTs, and (3) P25-graphene nanocomposites, respectively (Reproduced with permission from Ref. [104], Copyright © 2010 American Physical Society).

by Hou et al. demonstrated improved MB degradation. Compared with two-dimensional graphene, 3DG provides myriad conducting channels of very good conductivity to channel photogenerated electrons from TiO_2, which is beneficial for reducing electron-hole recombination [107]. A 3D network constructed by hydrothermal reactions and assembly of one-dimensional TiO_2 NW and two-dimensional graphene also has improved photocatalytic activity [108]. In summary, hybrids between conducting C-sp^2 networks and TiO_2 are advantageous for AOP applications because (1) the high electron conductivity of the nanocarbon-network support complements the high hole conductivity of TiO_2, and (2) the space-charge layer formed at the conjugation or chemically bonded interfaces between nanocarbon and TiO_2 provides an electrical bias for electron-hole separation.

Large scale applications of nanomaterials

Nanomaterial applications in AOP treatment are rapidly approaching reality thanks to the recent progress in large-scale, low-cost synthesis of all the key enabling nanomaterials, specifically BT and 3DG. Challenges nevertheless remain. In wastewater treatment plants, the challenge is to displace the existing technology, which will not happen unless the nanotechnology is compelling enough both in performance and in cost [6,109,110]. In water remediation field operations, the challenge is to cover a large water area of widely varying conditions and chemistry while achieving a high efficiency without the benefit of primary and secondary treatment and with minimum human intervention. Lifetime and recyclability are always a concern as they pertain to cost.

Large scale synthesis of 3D graphene

High-surface-area 3DG as a conducting and stand-alone catalytic support provides an attractive platform. For lower grade 3DG, large scale synthesis usually starts with GO, which can be produced inexpensively from naturally occurring graphite by Hummers' method [111]. Since GO is hydrophilic and easy to functionalize, dispersed GO sheets can be assembled into an aerogel [112]. For example, a hydrogel prepared in a protic solvent with the aid of cross-linkers or pH adjustment can provide an aerogel after gelation and freeze drying [113]. The aerogel is next reduced to 3D RGO to impart conductivity [92]. Other variations are possible. For example, chemical reduction, cross-linking and shape molding of GO sheets using a water/ammonia suspension under hydrothermal conditions have produced spongy graphene (SG) with a specific surface area of 430 $m^2 g^1$ [114]. The 3D RGO products from these high-throughput processes are rather inexpensive and excellent adsorbers for petroleum products, fats, and toxic solvents (Fig. 6a). For example, SG can absorb 20 to 85 times of its own weight, and as shown in Fig. 6b and c it can completely adsorb a dodecane contaminant from the water surface within 80 s. Since graphene is typically inert in air at below 600 °C, the adsorbates can be boiled off at a modest temperature, after which the sponge free of contaminant and structural damage may be used again (Fig. 6d).

The 3D RGO has a relatively low mechanical strength and poor electrical conductivity owing to the relatively low density of crosslinkers connecting the GO sheets. This problem is overcome by developing a CVD graphene, in which carbon is coated onto a sacrificial nano/mesoporous template; the template is later removed chemically [115]. The strength and conductivity of thus fabricated 3DG are template dependent because the only crosslinkers are nanocarbon crosslinks themselves with a spacing the same as template's pore size. Therefore, a template with a large pore size, such as commercially available Ni foam with μm pores, yields a fragile 3DG (3DG-Ni) once Ni is removed by acid etching (Fig. 7a, c) [116,117]. A sacrificial template such as Li_2CO_3 generated *in situ* by chemical reaction between Li_2O and CO was used to prepare 3DG with a honeycomb-like structure [118]. In contrast, a template of meso-

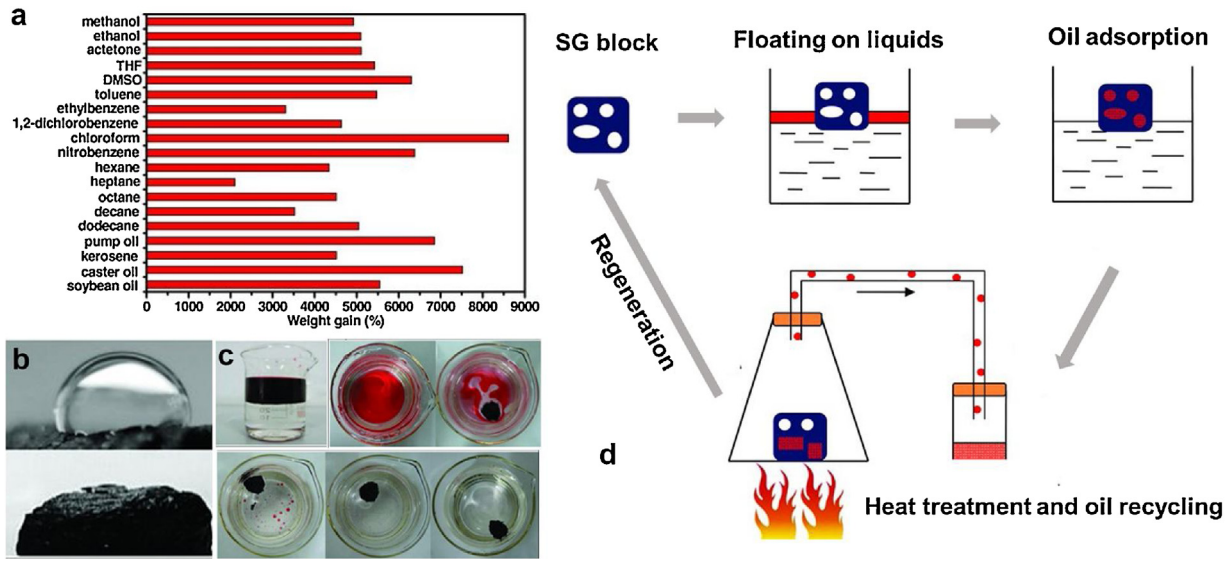

Fig. 6. (a) Adsorption capacity of SG for different liquid pollutants. (b) Non-wetting water droplet (top) versus rapid and complete adsorption of dodecane (bottom) on spongy graphene (SG). (c) SG adsorbing dodecane in simulated seawater contamination: rapid adsorption of floating dodecane by SG within 80 s, shown at intervals of 20 s. (d) Regeneration and reuse of SG for oil adsorption (Reproduced with permission from Ref. [114], Copyright © 2012 Wiley-VCH).

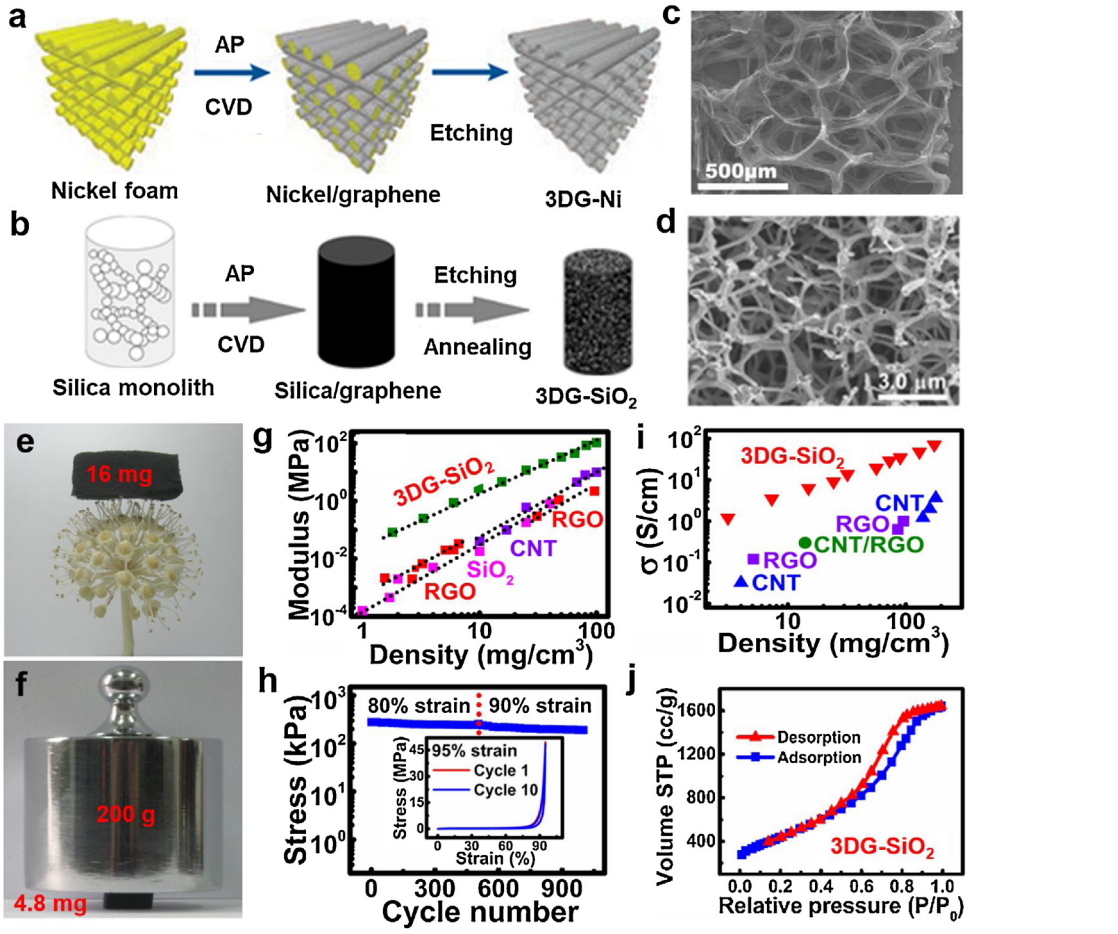

Fig. 7. CVD growth of 3D graphene (3DG) on (a) Ni foam and (b) silica monolith, followed by acid etching. SEM images of 3DG templated from (c) Ni foam (3DG-Ni) and (d) silica monolith (3DG-SiO_2). (e) A 10 cm^3 block of 3DG-SiO_2 (weight of 16 mg) on an umbel of *Fatsia japonica*. (f) 3DG-SiO_2 (weight of 4.8 mg) supporting a weight of 200 g without shape distortion. (g) Density versus small-strain modulus measured during 1 st compression cycle for 3DG-SiO_2, RGO aerogel, SiO_2 aerogel and aligned CNT film. (h) Compressive stress of 3DG-SiO_2 at 80% and 90% strain plotted versus cycle number. Inset: stress-strain loops cycled to 95% strain for 10 times. (i) Comparison of electrical conductivities of 3DG-SiO_2 with other ultralight carbon-based materials at several densities. (j) N_2 adsorption-desorption isotherms of 3DG-SiO_2 (Reproduced with permission from Ref. [23], Copyright © 2015 Wiley-VCH).

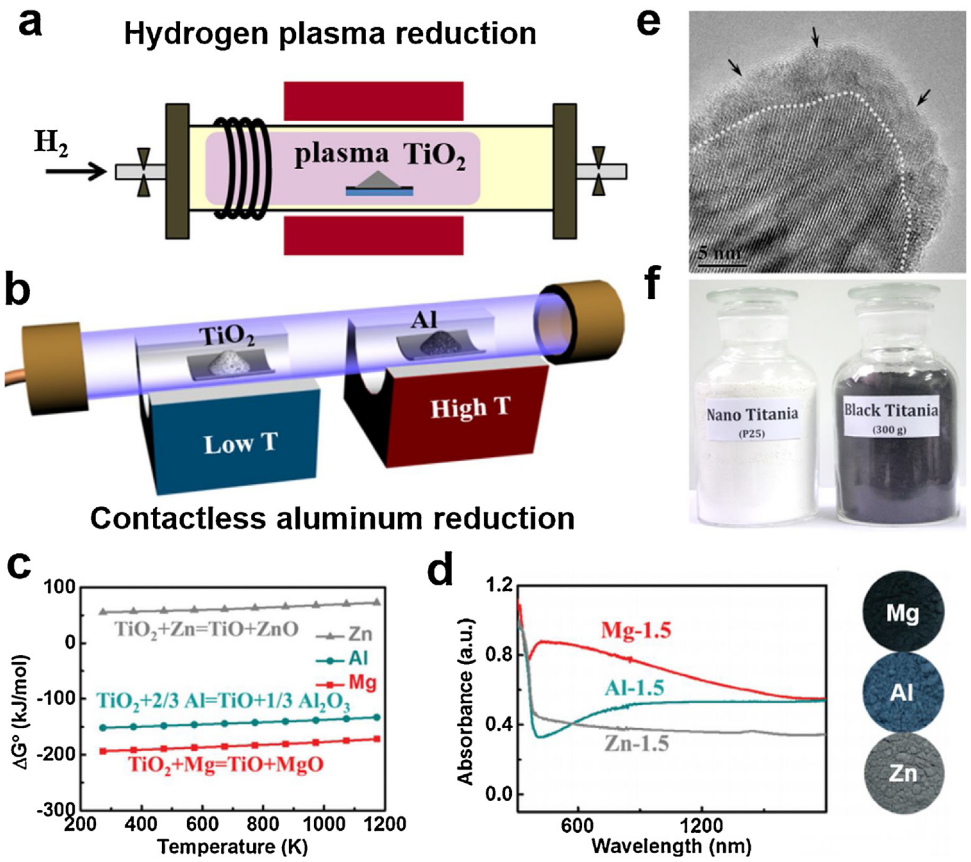

Fig. 8. (a) Hydrogen plasma reduction of P25 in a thermal plasma furnace. (b) Contactless Al-reduction of P25 in a two-zone furnace. (c) Calculated reaction Gibbs free energy of TiO_2 reduction by different metals (Mg, Al and Zn). (d) Absorption spectra and color appearance of P25 reduced by Mg, Al and Zn. (e) HRTEM image of TiO_{2-x} nanocrystal with crystalline-core disordered-shell microstructure. (f) BT (TiO_{2-x}) produced in 300 g batch by contactless Al-reduction.

porous SiO_2 aerogel—similar to synthetic zeolite—provides a highly robust and conductive 3DG (3DG-SiO_2) in which the SiO_2 template is again removed by HF acid etching after the CVD graphene is formed (Fig. 7b, d) [23,119]. (The SiO_2 aerogel is easily synthesized by preparing a water precursor that contains Pluronic block copolymer surfactants and silica sources, followed by hydrothermal treatment and calcination.) A 10 cm^3 block of ultralight 3DG weighing 16 mg can be supported on an umbel of Fatsia japonica (Fig. 7e), and it takes the form of a tetrahedrally connected tubular graphene network which maintains continuous, covalent C-sp^2 bonding. Such structure endows 3DG high strength, excellent conductivity and indeed superelasticity, as Fig. 7f-i shows how a 3DG can completely recover the shape and microstructure after 99% compression once the load is off. Being much more than 99% porous, this 3DG is completely transparent to liquid despite a very high specific surface area of ~1,000 cm^2 g^1 (Fig. 7j), which makes possible rapid soaking and adsorption. The 3DG also exhibits excellent recycling ability: rapid oil adsorption in 2 s, followed by combustion burn-off of oil, then ready for oil adsorption again [23]. Further doping the 3DG can alter the surface property without adversely affecting conductivity. For example, pyrrolic and pyridinic N change the 3DG surfaces from a hydrophobic one to a hydrophilic one, resulting in a large enhancement in redox activity without affecting conductivity [120]. In addition, N doping is reportedly beneficial for the adsorption of positively-charged dye or metal ions through the chelation effect of N dopant whose unpaired electrons can electrostatically interact with these ions [121,122]. Lastly, inexpensive sol-gel silica can too be used as the template, and the cost can be further reduced by performing CVD at below 1000 °C, which is the path our group used to produce inexpensive 3DG in large quantity.

Large scale synthesis of black titania

BT enjoys full-spectrum solar absorption and is much more photocatalytically active than the "gold-standard" photocatalyst P25, which is a commercially available white titania. Several production processes have been developed for BT, of which two methods illustrated in Fig. 8a-b are most noteworthy for their simplicity. While BT (HP-TiO_2) was originally synthesized by treating P25 under high-pressure H_2 at about 200 °C for 5 days, BT ($TiO_{2-x}H_x$) of greatly improved solar absorption (83%) can be made by a much faster process of hydrogen plasma treatment that converts P25 into BT in 4-8 h at 500 °C (Fig. 8**a**) [62,64]. Its nanoparticle with the desired crystalline-core disordered-shell microstructure displays superior photocatalytic activity and remarkable cycling stability for repeated MO degradation. To further simplify synthesis and to conform to conventional powder processing, one can substitute gaseous/plasma hydrogen by hydrides powders (such as $NaBH_4$, N_2H_4, CaH_2, TiH_2, etc.), which are added to the starting powders and later release molecular hydrogen under mild calcination conditions [69,123,124]. For example, a gel made from a TiO_2 sol with $NaBH_4$ addition is converted to BT in 1.5 h calcination at 500 °C in Ar. This process can produce BT in 100 g batches. However, the product needs washing to remove residual Na [125].

Thermodynamically, reduction can also be achieved without hydrogen. From the oxidation free energies in the Ellingham diagram, one can plot the reaction Gibbs free energy in Fig. 8c indicating that TiO_2 can be reduced by Al, and Mg [126]. This was experimentally verified. (Fig. 8c also predicts that Zn cannot reduce TiO_2, which was too verified experimentally.) Mg-reduction proved to be easily controllable and yielded BT with much higher solar

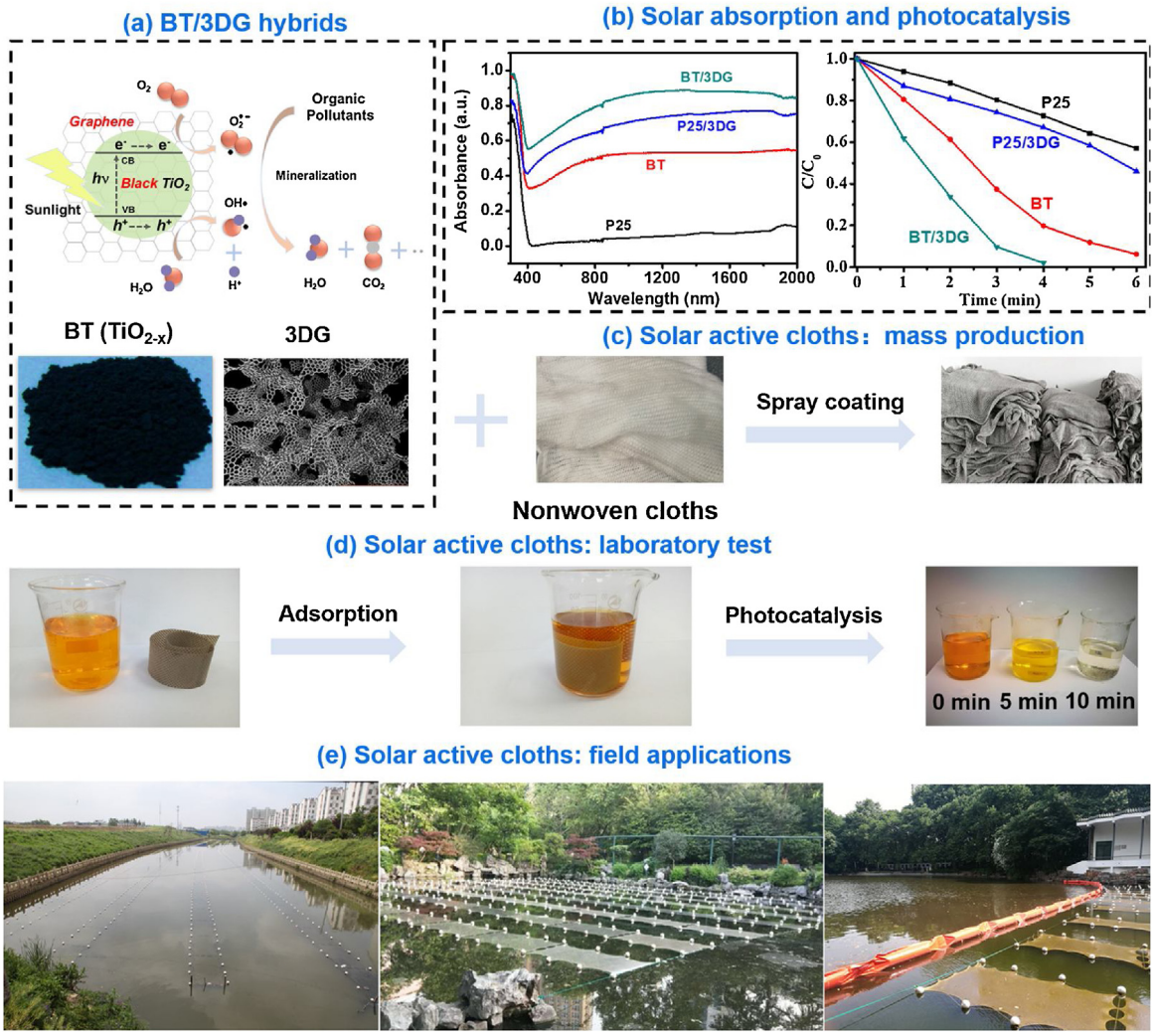

Fig. 9. (a) Schematic illustration of BT/3DG hybrids for photocatalytic organic pollutant decomposition. (b) Absorption spectra of P25, BT (TiO_{2-x}), P25/3DG and BT/3DG, and their photocatalytic performances for methyl orange (MO) degradation. (All photocatalysts in their powder form.) (c) Immobilization of BT/3DG hybrids on nonwoven cloth, forming solar active cloths. (d) Photocatalytic degradation of MO over one piece of solar active cloths in laboratory test. (e) Solar active cloths deployed on polluted rivers and ponds for large-scale wastewater treatment.

absorbance (Fig. 8d). In one protocol, commercial P25 mixed with Mg powders in a sealed quartz tube produces BT after calcination for 10 h at 500 °C. However, the product again needs washing, by weak acid, to remove residual Mg and MgO.

To further simplify the process, our group separated metal reductants and white TiO_2 and placed them in separate zones of a two-zone furnace, respectively (Fig. 8b) [65]. In this way, Al powders heated to 800 °C in the high-temperature zone can consume oxygen from the low-temperature zone where white TiO_2 is converted to BT (TiO_{2-x}) after 6 h in a base pressure of < 0.5 Pa. This process requires no powder mixing and product washing, and the BT obtained also has the desired crystalline-core (anatase) disordered-shell microstructure (Fig. 8e), outstanding solar absorption characteristics and excellent photocatalytic activity. The as-prepared BT shows high stability in air for several months, and it is oxidized to white TiO_2 at above 300 °C. Currently, this process routinely supplies mass-produced BT for the large-scale water treatment projects undertaken by our group (Fig. 8f).

Field applications

Practical water-treatment applications on a large scale require a large quantity of low-cost nanomaterials that are stable thermally, chemically and photochemically. Commercially available white titania P25 mostly satisfies these requirements, but BT with a relatively similar cost and a much improved photocatalytic performance is clearly a better choice. To reduce cost further, the nanomaterials should last for a long time, and be easily recoverable after that. In this respect, the BT/3DG construct (Fig. 9a) is particularly desirable in that it immobilizes BT on a high-surface-area 3DG support, thus providing preconcentration and synergistically enhanced photocatalytic activity, as well as a robust form factor that allows easy solid-liquid separation and recovery. Specifically, when TiO_{2-x} is used for BT in BT/3DG, it exhibits superior light harvesting and photocatalytic activity compared to P25, P25/3DG hybrids, or BT alone; for example, photodegradation of MO over BT/3DG powders is completed in 4 min (Fig. 9b).

To bring BT/3DG to field applications, our group has developed a solar active cloth in which BT/3DG hybrids are bonded to a nonwoven cloth by a polymeric binder (Fig. 9c). This solar active cloth caused MO photodegradation in 10 min (Fig. 9d). The cloth is buoyant and floats on water. Field tests for water remediation have been conducted at multiple locations, including rivers, lakes, and ponds in municipal parks (Fig. 9e). Typically, two weeks after the cloths are deployed, a significant reduction of TOC, nitrogen and phosphorus components of the treated water is measured, and a very

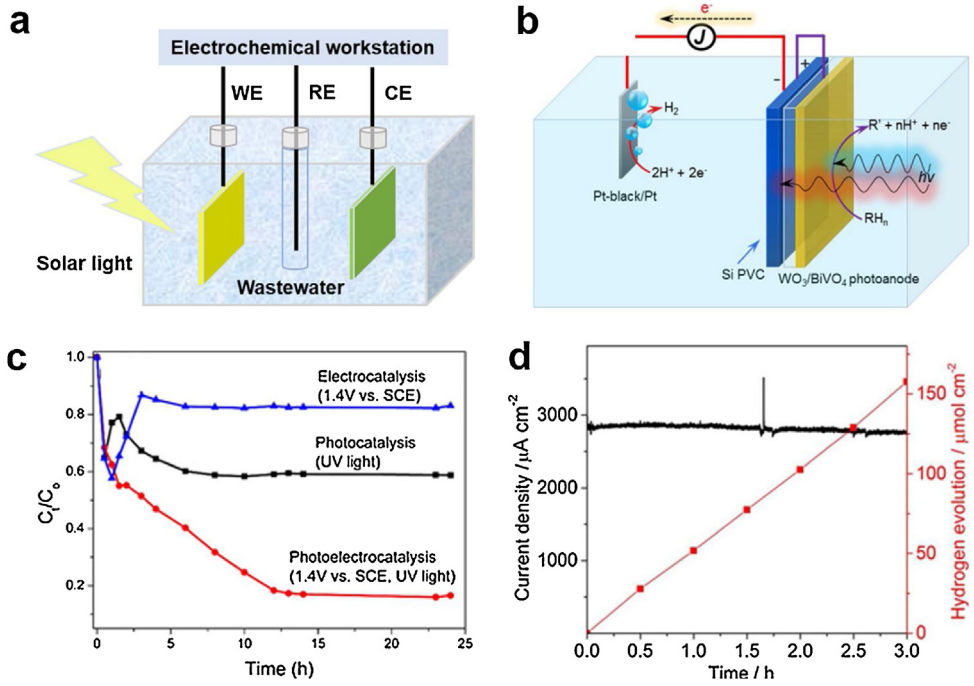

Fig. 10. (a) The setup of a voltage assisted photoelectrocatalytic (PEC) unit for wastewater treatment; it includes a reference electrode (saturated calomel electrode, SCE), a counter electrode (Pt electrode) and a working electrode (solar-active semiconductors). (b) Schematic illustration of a self-sustaining monolithic PEC/photovoltaic (PV) system for simultaneous organic-containing wastewater treatment, hydrogen generation and electricity production (Reproduced with permission from Ref. [137], Copyright © 2018 Elsevier). (c) Comparison of degradation activity by electrocatalytic (1.4 V vs. SCE), photocatalytic (UV light), and PEC process (1.4 V vs. SCE, UV light) using a titania-graphene hydrogel (TGH) as a working electrode (Reproduced with permission from Ref. [133], Copyright © 2017 Elsevier). (d) Photocurrent-time curve and hydrogen evolution rate of the PEC/PV hybrid system (Reproduced with permission from Ref. [137], Copyright © 2018 Elsevier).

visible change in the appearance of water, e.g., from turbid to clear, is produced. This is all the more remarkable in that it is achieved without the aid of primary and secondary treatment. So, the solar active cloths, containing BT and 3DG that are usually considered good for AOP only, can actually accomplish water remediation by themselves. To date, 8 tons of black titania and 100 kg of 3DG have been used to fabricate solar active cloths that have been deployed to successfully remediate 600 acres of polluted water at four sites in China (the Dingguang River in Anhui province, Huanglei River in Shandong province, Zhongshan Park and Tianshan Park in Shanghai city). These numbers are growing rapidly since the inception of the project in Spring 2018, attesting to the initial success of the technology.

Lifetime and recycling

Lifetime and recycling are pertaining to the cost of water treatment, which is of paramount importance for large-scale applications. Clearly, chemical and physical stability under prolong sunlight exposure is the first prerequisite. In this respect, the proven stability and antifouling ability of TiO_2 nanoparticles are encouraging: they can withstand weathering as demonstrated in various paints, coatings, glasses, cement, tiles, and other products over the last 20 years. However, a definitive assessment is still needed for BT because colored TiO_2 does convert to white TiO_2 over time under ambient condition. Meanwhile, BT/3DG-bearing cloths on which BT and 3DG are immobilized are evidently recoverable. However, immobilization comes with some penalty, in that the immobilized BT/3DG hybrids manifest lower photocatalytic activities than powdered/granular BT/3DG that has a higher exposure area to water and sunlight in addition to better local electrical conductivity. So it would be very desirable to engineer an improved product that allows easy deployment and recovery while maintaining excellent photocatalytic performance. To aid separation and recovery, one possibility is to introduce magnetic beads that are already used for similar purposes in industrial and medical technologies. Magnetic particles come in both ferromagnetic/metallic and ferromagnetic/insulating-oxide varieties [127,128]. (The latter include hematite Fe_2O_3, magnetite Fe_3O_4, and various ferrites MFe_2O_4, M = Mg, Ni, Zn, Cu, etc.) Since some of these oxides are themselves semiconductors with good visible light absorption and photocatalytic properties, it is conceivable that they could be incorporated into the BT/3DG hybrids to further promote the overall degradation efficiency while improving lifetime and recyclability. In short, any advance in lifetime and recyclability is likely to have a major impact on the overall cost of nanomaterial-based water treatment and remediation.

Advanced water treatment technologies

As mentioned previously, electron-hole separation is important for achieving high photocatalytic activity; this also holds for photovoltaic efficiency. An internal field can drive electron and hole separation in the opposite directions, but an external electrical field is even more effective. Although introducing an external field to (free) powders is a daunting task, it becomes straightforward if all the photocatalyst nanoparticles are already in firm contact with a conducting support. In this configuration, external-field driven electron-hole separation is easily achieved and the carrier current flowing in the external circuit can drive a load for other purposes—for example, water splitting and hydrogen (fuel) production. This is the concept of photocatalytic fuel cell (PFC) [129].

Of course, to operate a PFC, a voltage source is needed. But this too can be solar driven by a photovoltaic cell (PVC). Indeed, with a slight reconfiguration, the construct used for photocatalytic AOP can be adapted for PVC with the same solar-active materials (e.g., P25 and BT). Such combination of PFC and photocatalysis (PC) may

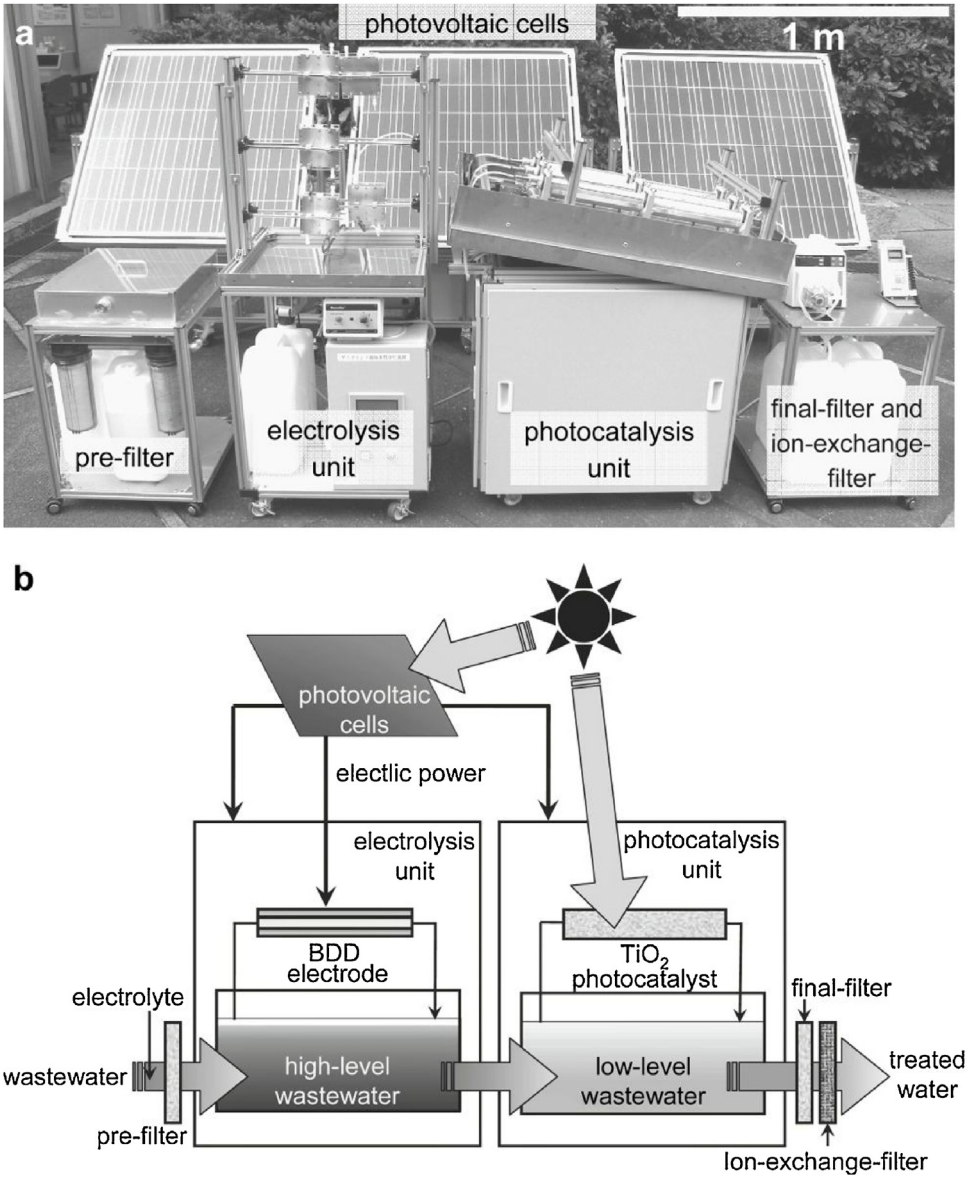

Fig. 11. (a) The setup of an integrated wastewater treatment system, which consists of an electrolysis unit and a photocatalysis unit. (b) Working principle of the system (Reproduced with permission from Ref. [138], Copyright © 2010 Elsevier).

be termed photoelectrocatalysis (PEC) [130,131]. A simple PEC unit consists of a reference electrode (saturated calomel electrode, etc.), a counter electrode (Pt foil, etc.) and a working electrode, with an external voltage provided by an electrochemical workstation, a PVC, or another galvanic source (Fig. 10a). Lastly, the three devices, PC, PFC, and PVC can be integrated into an advanced, multitasking module that performs water treatment, energy generation, and possibly energy storage (Fig. 10b).

These concepts have been demonstrated. Vinodgopal et al. first reported the benefit of an external bias that enhances electron-hole separation in the photodegradation of 4-chlorophenol by a TiO_2 thin film deposited on an electrode [132]. The process benefited from an external bias potential because of enhanced electron-hole separation. PEC cells using other semiconductors (ZnO, WO_3, Fe_2O_3, Bi_2WO_6, $BiPO_4$, etc.) have also successfully caused deep mineralization of refractory organic pollutants. [130] Recently, a PEC unit using a titania-graphene hydrogel (TGH) supported on a stainless steel working electrode has been built to demonstrate efficient degeneration of MB [133]. The MB degradation rate of this PEC unit was 2 times higher than that of a stand-alone photocatalysis unit, and 4.7 times higher than that of a stand-alone electrocatalysis unit (Fig. 10c). Therefore, the synergistic advantage of applying an external voltage during photoexcitation in electrocatalysis and photocatalysis is firmly established.

A dual PFC unit coupling a TiO_2 photoanode and a Cu_2O photocathode has also been used to realize simultaneous phenol photodegradation and hydrogen production [134]. Other combinations using WO_3/Cu_2O, $BiVO_4@TiO_2/ZnO@CuO$, $BiVO_4@WO_3@W/Pt@Si$ were also studied [135,136]. With a rear Si PVC, a fluorine-doped tin oxide (FTO) supported $BiVO_4@WO_3$ photoanode and a Pt-black counter electrode (CE), Zeng et al. constructed a self-sustaining monolithic PEC/PV hybrid system (Fig. 10b) [137]. Under sunlight illumination, photodegradation of organic pollutants and photocurrent production occur on the $BiVO_4@WO_3$ photoanode where higher energy photons are absorbed. Meanwhile, the rear Si cell absorbing lower energy photons generates a bias potential to drive the transfer of photogenerated electrons from the photoanode to the Pt CE for hydrogen production (Fig. 10d).

Finally, we describe a solar-cell powered integrated system that treats polluted water from river [138]. It consists of an electrolysis unit, a photocatalysis unit and several PVCs (Fig. 11). High-level wastewater is electrochemically treated in a boron-doped diamond electrode to obtain low-level wastewater, which is further degraded by TiO_2 photocatalysts. After an additional filtration step in which water passes through a final filter and several ion-exchange-filter units, most of the chemical and biological contaminants are removed: the COD value decreases from 106.1 mg L^1 to less than 1.0 mg L^1.

Conclusions

Significant progress in developing nanomaterials for water treatment has been made in the last decade. Among many accomplishments, the most notable two are (a) the discovery of black titania capable of full solar spectrum photon absorption and (b) the innovation in constructing three dimensional nanocarbon combining excellent electrical conductivity and high surface area with remarkable mechanical flexibility and integrity. The utility of these nanomaterials has been demonstrated in large-scale water remediation projects that use hybrids of BT and 3DG, engineered into a practical format of photocatalytic cloths. Further nanotechnology advances in this direction look promising and will benefit from advances in the following areas.

Adsorption of 3DG: To suit a wide variety of pollutants of different sizes, compositions and physical chemistry, different subclasses of 3DG with tailored pore volumes, pore size distributions and surface functional groups/heteroatom doping are needed. This will require additional insight in pollutant adsorption on 3DG.

Band structure tailoring of BT: Notwithstanding full-spectrum light absorption of BT, the photoactivity in the visible and near infrared region is still unsatisfactory. Further manipulation of band edge positions to promote efficient utilization of lower energy photons may be possible, which will improve overall photocatalytic efficiency.

Design of interfaces and surfaces: While the BT/3DG hybrids already combine excellent full-spectrum absorption of BT and excellent conductivity and surface activity of 3DG, the BT/3DG interface and the Ti-O-C bonds should be optimized to further facilitate electron transfer and system photoactivity. Striking a balance between high surface area and high overall conductivity may also be needed.

Degradation of nanomaterials: The long-term stability of BT and BT/3DG hybrids in various water chemistries is clearly important and should be evaluated.

Acknowledgements

FQH and WZ acknowledge the financial support from the National key R&D Program of China (Grant No. 2016YFB0901600), the National Natural Science Foundation of China (Grand No.Y93GJ11101), the Key Research Program of Chinese Academy of Sciences (Grants No. QYZDJ-SSW-JSC013 and KGZD-EW-T06), and the Innovation Project of Shanghai Institute of Ceramics (Grant No. Y73ZC6160G).

References

[1] F.R. Rijsberman, Agr. Water Manage. 80 (2006) 5–22.
[2] WHO World Water Day Report, World Health Organization, Geneva, 2019 https://www.who.int/water_sanitation_health/takingcharge.html.
[3] L. Haller, G. Hutton, J. Bartram, J. Water Health 5 (2007) 467–480.
[4] J. Alcamo, T. Henrichs, T. Rosch, World water in 2025: global modeling and scenario analysis, in: F.R. Rijsberman (Ed.), World Water Scenarios Analyses, World Water Council, Marseille, France, 2000.
[5] Guidelines for drinking-water quality: fourth edition incorporatiog the first addendum: World Health Organisation; 2015. Licence: CC BY-NC-SA 3.0IGO.
[6] P.J.J. Alvarez, C.K. Chan, M. Elimelech, N.J. Halas, D. Villagrán, Nat. Nanotech. 13 (2018) 634–641.
[7] Primer for Municipal Wastewater Treatment Systems, United States Environmental Protection Agency, Washington, 2019 https://www.epa.gov/npdes/npdes-resources.
[8] O. Legrini, E. Oliveros, A.M. Braun, Chem. Rev. 93 (1993) 671–698.
[9] R. Li, L. Zhang, P. Wang, Nanoscale 7 (2015) 17167–17194.
[10] X. Chen, S.S. Mao, Chem. Rev. 107 (2007) 2891–2959.
[11] K. Yang, B. Xing, Chem. Rev. 110 (2010) 5989–6008.
[12] N.R. Khalid, A. Majid, M.B. Tahir, N.A. Niaz, S. Khalid, Ceram. Int. 43 (2017) 14552–14571.
[13] A.G. Fane, R. Wang, M.X. Hu, Angew. Chem. Int. Ed. 54 (2015) 3368–3386.
[14] A. Dąbrowski, Adv. Colloid Inter. Sci. 93 (2001) 135–224.
[15] M.T. Yagub, T.K. Sen, S. Afroze, H.M. Adv. Colloid Inter. Sci. 209 (2014) 172–184.
[16] W. Steele, Chem. Rev. 93 (1993) 2355–2378.
[17] F. Rouquerol, J. Rouquerol, K. Sing. Adsorption by Powders and Porous Solids, Academic Press, London, 1999, pp. 448–459.
[18] H. Sontheimer, J.C. Crittenden, R.S. Summers, Activated Carbon for Water Treatment, DVGW Forschungsstelle Engler-Bunte Institut, Karlsruhe, 1988.
[19] H. Marsh, F.R. Reinoso. Activated Carbon, Elsevier, Amsterdam, 2006.
[20] K.S. Novoselov, A.K. Geim, S.V. Morozov, D. Jiang, Y. Zhang, S.V. Dubonos, I.V. Grigorieva, A.A. Firsov, Science 306 (2004) 666–669.
[21] A.K. Geim, K.S. Novoselov, Nat. Mater. 6 (2007) 183.
[22] A.H. Castro Neto, F. Guinea, N.M.R. Peres, K.S. Novoselov, A.K. Geim, Rev. Mod. Phys. 81 (2009) 109–162.
[23] H. Bi, I.-W. Chen, T. Lin, F. Huang, Adv. Mater. 27 (2015) 5943–5949.
[24] U.N. Maiti, W.J. Lee, J.M. Lee, Y. Oh, J.Y. Kim, J.E. Kim, J. Shim, T.H. Han, S.O. Kim, Adv. Mater. 26 (2014) 40–67.
[25] A. Bhatnagar, W. Hogland, M. Marques, M. Sillanpää, Chem. Eng. J. 219 (2013) 499–511.
[26] V.K. Gupta, T.A. Saleh, Environ. Sci. Pollut. Res. 20 (2013) 2828–2843.
[27] J. Liu, N.P. Wickramaratne, S.Z. Qiao, M. Jaroniec, Nat. Mater. 14 (2015) 763.
[28] P. Zhang, L. Wang, S. Yang, J.A. Schott, X. Liu, S.M. Mahurin, C. Huang, Y. Zhang, P.F. Fulvio, M.F. Chisholm, S. Dai, Nat. Commun. 8 (2017) 15020.
[29] S. Gao, X. Li, L. Li, X. Wei, Nano Energy 33 (2017) 334–342.
[30] P. Pachfule, D. Shinde, M. Majumder, Q. Xu, Nat. Chem. 8 (2016) 718.
[31] J. Rivera-Utrilla, M. Sánchez-Polo, V. Gómez-Serrano, P.M. Álvarez, M.C.M. Alvim-Ferraz, J.M. Dias, J. Hazard. Mater. 187 (2011) 1–23.
[32] Y.F. Jia, K.M. Thomas, Langmuir 16 (2000) 1114–1122.
[33] W. Wei, C. Yu, Q. Zhao, G. Li, Y. Wan, Chem. Eur. J. 19 (2013) 566–577.
[34] I. Velo-Gala, J.J. López-Peñalver, M. Sánchez-Polo, J. Rivera-Utrilla, Appl. Catal. B: Environ. 207 (2017) 412–423.
[35] H.-J. Lu, J.-K. Wang, S. Ferguson, T. Wang, Y. Bao, H.-x. Hao, Nanoscale 8 (2016) 9962–9975.
[36] J.J. Pignatello, E. Oliveros, A. MacKay, Crit. Rev. Environ. Sci. Technol. 36 (2006) 1–84.
[37] E. Neyens, J. Baeyens, J. Hazard. Mater. 98 (2003) 33–50.
[38] R.R. Gadkari, S.W. Ali, R. Alagirusamy, A. Das, Silver Nanoparticles in Water Purification: Opportunities and Challenges, Springer International Publishing, Cham, 2018, pp. 229–237.
[39] M.N. Chong, B. Jin, C.W.K. Chow, C. Saint, Water Res. 44 (2010) 2997–3027.
[40] J.M. Herrmann, C. Guillard, P. Pichat, Catal. Today 17 (1993) 7–20.
[41] A. Fujishima, T.N. Rao, D.A. Tryk, J. Photochem. Photobiol., C: Photochem. Rev. 1 (2000) 1–21.
[42] U.I. Gaya, A.H. Abdullah, J. Photochem. Photobiol., C: Photochem. Rev. 9 (2008) 1–12.
[43] M.R. Hoffmann, S.T. Martin, W. Choi, D.W. Bahnemann, Chem. Rev. 95 (1995) 69–96.
[44] A. Mills, R.H. Davies, D. Worsley, Chem. Soc. Rev. 22 (1993) 417–425.
[45] H. Gerischer, A. Heller, J. Phys. Chem. 95 (1991) 5261–5267.
[46] M. Pelaez, N.T. Nolan, S.C. Pillai, M.K. Seery, P. Falaras, A.G. Kontos, P.S.M. Dunlop, J.W.J. Hamilton, J.A. Byrne, K. O'Shea, M.H. Entezari, D.D. Dionysiou, Appl. Catal. B: Environ. 125 (2012) 331–349.
[47] N. Takeno, Geological Survey of Japan Open File Report, 419, 2005, pp. 102.
[48] L.M. Pastrana-Martínez, S. Morales-Torres, S.K. Papageorgiou, F.K. Katsaros, G.E. Romanos, J.L. Figueiredo, J.L. Faria, P. Falaras, A.M.T. Silva, Appl. Catal. B: Environ. 142-143 (2013) 101–111.
[49] G. Balasubramanian, D.D. Dionysiou, M.T. Suidan, I. Baudin, J.-M. Laîné, Appl. Catal. B: Environ. 47 (2004) 73–84.
[50] H. Kisch, Angew. Chem. Int. Ed. 52 (2013) 812–847.
[51] J. Schneider, M. Matsuoka, M. Takeuchi, J. Zhang, Y. Horiuchi, M. Anpo, D.W. Bahnemann, Chem. Rev. 114 (2014) 9919–9986.
[52] H. Park, Y. Park, W. Kim, W. Choi, J. Photochem. Photobiol., C: Photochem. Rev. 15 (2013) 1–20.
[53] S. Shen, J. Chen, M. Wang, X. Sheng, X. Chen, X. Feng, S.S. Mao, Prog. Mater. Sci. 98 (2018) 299–385.
[54] X.Y. Liu, G.L. Zhu, X. Wang, X.T. Yuan, T.Q. Lin, F.Q. Huang, Adv. Energy Mater. 6 (2016).
[55] X.B. Chen, L. Liu, F.Q. Huang, Chem. Soc. Rev. 44 (2015) 1861–1885.
[56] Y. Ma, X. Wang, Y. Jia, X. Chen, H. Han, C. Li, Chem. Rev. 114 (2014) 9987–10043.
[57] D. Dvoranová, V. Brezová, M. Mazúr, M.A. Malati, Appl. Catal. B: Environ. 37 (2002) 91–105.

[58] T. Umebayashi, T. Yamaki, H. Itoh, K. Asai, J. Phys. Chem. Solids 63 (2002) 1909–1920.
[59] X. Chen, C. Burda, J. Am. Chem. Soc. 130 (2008) 5018–5019.
[60] S. Sakthivel, M.V. Shankar, M. Palanichamy, B. Arabindoo, D.W. Bahnemann, V. Murugesan, Water Res. 38 (2004) 3001–3008.
[61] Y. Bessekhouad, D. Robert, J.V. Weber, Catal. Today 101 (2005) 315–321.
[62] X. Chen, L. Liu, P.Y. Yu, S.S. Mao, Science (2011) 746–749.
[63] A. Sinhamahapatra, J.P. Jeon, J.S. Yu, Energy Environ. Sci. 8 (2015) 3539–3544.
[64] Z. Wang, C.Y. Yang, T.Q. Lin, H. Yin, P. Chen, D.Y. Wan, F.F. Xu, F.Q. Huang, J.H. Lin, X.M. Xie, M.H. Jiang, Adv. Funct. Mater. 23 (2013) 5444–5450.
[65] Z. Wang, C.Y. Yang, T.Q. Lin, H. Yin, P. Chen, D.Y. Wan, F.F. Xu, F.Q. Huang, J.H. Lin, X.M. Xie, M.H. Jiang, Energy Environ. Sci. 6 (2013) 3007–3014.
[66] C. Yang, Z. Wang, T. Lin, H. Yin, X. Lü, D. Wan, T. Xu, C. Zheng, J. Lin, F. Huang, X. Xie, M. Jiang, J. Am. Chem. Soc. 135 (2013) 17831–17838.
[67] H.L. Cui, W. Zhao, C.Y. Yang, H. Yin, T.Q. Lin, Y.F. Shan, Y. Xie, H. Gu, F.Q. Huang, J. Mater. Chem. A 2 (2014) 8612–8616.
[68] G.L. Zhu, T.Q. Lin, X.J. Lu, W. Zhao, C.Y. Yang, Z. Wang, H. Yin, Z.Q. Liu, F.Q. Huang, J.H. Lin, J. Mater. Chem. A 1 (2013) 9650–9653.
[69] G. Zhu, Y. Shan, T. Lin, W. Zhao, J. Xu, Z. Tian, H. Zhang, C. Zheng, F. Huang, Nanoscale 8 (2016) 4705–4712.
[70] W. Zhou, W. Li, J.-Q. Wang, Y. Qu, Y. Yang, Y. Xie, K. Zhang, L. Wang, H. Fu, D. Zhao, J. Am. Chem. Soc. 136 (2014) 9280–9283.
[71] Y.H. Hu, Angew. Chem. Int. Ed. 51 (2012) 12410–12412.
[72] M.A. Green, J. Xu, H. Liu, J. Zhao, K. Li, L. Liu, H. Qin, Y. Zhu, D. Shen, X. Chen, Mater. Today Phys. 4 (2018) 64–69.
[73] L. Tian, J. Xu, M. Just, M. Green, L. Liu, X. Chen, J. Mater. Chem. C 5 (2017) 4645–4653.
[74] T.Q. Lin, C.Y. Yang, Z. Wang, H. Yin, X.J. Lu, F.Q. Huang, J.H. Lin, X.M. Xie, M.H. Jiang, Energy Environ. Sci. 7 (2014) 967–972.
[75] T. Hisatomi, J. Kubota, K. Domen, Chem. Soc. Rev. 43 (2014) 7520–7535.
[76] R. Marschall, Adv. Funct. Mater. 24 (2014) 2421–2440.
[77] L. Guan, X. Chen, ACS Appl. Energy Mater. 1 (2018) 4313–4320.
[78] K.V. Vokhmintcev, P.S. Samokhvalov, I. Nabiev, Nano Today 11 (2016) 189–211.
[79] H. Wang, L. Zhang, Z. Chen, J. Hu, S. Li, Z. Wang, J. Liu, X. Wang, Chem. Soc. Rev. 43 (2014) 5234–5244.
[80] J. Li, L. Cai, J. Shang, Y. Yu, L. Zhang, Adv. Mater. 28 (2016) 4059–4064.
[81] G. Zhang, H. Wu, G. Li, Q. Huang, C. Yang, F. Huang, F. Liao, J. Lin, Sci. Rep. 3 (2013) 1265.
[82] I. Grinberg, D.V. West, M. Torres, G. Gou, D.M. Stein, L. Wu, G. Chen, E.M. Gallo, A.R. Akbashev, P.K. Davies, J.E. Spanier, A.M. Rappe, Nature 503 (2013) 509.
[83] X. Lin, F. Huang, W. Wang, Y. Wang, Y. Xia, J. Shi, Appl. Catal. A: General 313 (2006) 218–223.
[84] Z. Shan, Y. Wang, H. Ding, F. Huang, J. Mol. Cata. A: Chemical 302 (2009) 54–58.
[85] X. Lin, J. Wu, X. Lü, Z. Shan, W. Wang, F. Huang, Phys. Chem. Chem. Phys. 11 (2009) 10047–10052.
[86] J. Wu, F. Huang, Z. Shan, Y. Wang, Dalton Trans. 40 (2011) 6906–6911.
[87] K.-L. Zhang, C.-M. Liu, F.-Q. Huang, C. Zheng, W.-D. Wang, Appl. Catal. B: Environ. 68 (2006) 125–129.
[88] J.B. Goodenough, J.S. Zhou, Chem. Mater. 10 (1998) 2980–2993.
[89] M.-Q. Yang, N. Zhang, M. Pagliaro, Y.-J. Xu, Chem. Soc. Rev. 43 (2014) 8240–8254.
[90] Q. Xiang, J. Yu, M. Jaroniec, Chem. Soc. Rev. 41 (2012) 782–796.
[91] O.C. Compton, S.T. Nguyen, Small 6 (2010) 711–723.
[92] C.K. Chua, M. Pumera, Chem. Soc. Rev. 43 (2014) 291–312.
[93] M. Asiltürk, Ş. Şener, Chem. Eng. J. 180 (2012) 354–363.
[94] Y. Yao, G. Li, S. Ciston, R.M. Lueptow, K.A. Gray, Environ. Sci. Technol. 42 (2008) 4952–4957.
[95] Y. Chuan-Yu, L. Yu-Feng, H. Chih-Hung, T. Yao-Hsuan, M.M. Chen-Chi, C. Min-Chao, S. Hsin,Nanotechnology 19 (2008), 045604.
[96] B. Gao, G.Z. Chen, G. Li Puma, Appl. Catal. B: Environ. 89 (2009) 503–509.
[97] K. Woan, G. Pyrgiotakis, W. Sigmund, Adv. Mater. 21 (2009) 2233–2239.
[98] B. Qiu, Y. Zhou, Y. Ma, X. Yang, W. Sheng, M. Xing, J. Zhang, Sci. Rep. 5 (2015) 8591.
[99] L. Li, L. Yu, Z. Lin, G. Yang, ACS Appl. Mater. Inter. 8 (2016) 8536–8545.
[100] S. Cao, T. Liu, Y. Tsang, C. Chen, Appl. Surf. Sci. 382 (2016) 225–238.
[101] M. Xing, X. Li, J. Zhang, Sci. Rep. 4 (2014) 5493.
[102] W. Fang, M. Xing, J. Zhang, J. Photochem. Photobiol., C: Photochem. Rev. 32 (2017) 21–39.
[103] G. Williams, B. Seger, P.V. Kamat, ACS Nano 2 (2008) 1487–1491.
[104] H. Zhang, X. Lv, Y. Li, Y. Wang, J. Li, ACS Nano 4 (2010) 380–386.
[105] K. He, G. Chen, G. Zeng, A. Chen, Z. Huang, J. Shi, T. Huang, M. Peng, L. Hu, Appl. Catal. B: Environ. 228 (2018) 19–28.
[106] C. Li, G. Shi, Nanoscale 4 (2012) 5549–5563.
[107] C. Hou, Q. Zhang, Y. Li, H. Wang, J. Hazard. Mater. 205-206 (2012) 229–235.
[108] X. Pan, Y. Zhao, S. Liu, C.L. Korzeniewski, S. Wang, Z. Fan, ACS Appl. Mater. Inter. 4 (2012) 3944–3950.
[109] D. Jassby, T.Y. Cath, H. Buisson, Nat. Nanotech. 13 (2018) 670–672.
[110] B.C. Hodges, E.L. Cates, J.-H. Kim, Nat. Nanotech. 13 (2018) 642–650.
[111] D.C. Marcano, D.V. Kosynkin, J.M. Berlin, A. Sinitskii, Z. Sun, A. Slesarev, L.B. Alemany, W. Lu, J.M. Tour, ACS Nano 4 (2010) 4806–4814.
[112] D.R. Dreyer, S. Park, C.W. Bielawski, R.S. Ruoff, Chem. Soc. Rev. 39 (2010) 228–240.
[113] Y. Xu, K. Sheng, C. Li, G. Shi, ACS Nano 4 (2010) 4324–4330.
[114] H. Bi, X. Xie, K. Yin, Y. Zhou, S. Wan, L. He, F. Xu, F. Banhart, L. Sun, R.S. Ruoff, Adv. Funct. Mater. 22 (2012) 4421–4425.
[115] K. Chen, L. Shi, Y. Zhang, Z. Liu, Chem. Soc. Rev. 47 (2018) 3018–3036.
[116] Z. Chen, W. Ren, L. Gao, B. Liu, S. Pei, H.-M. Cheng, Nat. Mater. 10 (2011) 424.
[117] Z. Xia, D. Wei, E. Anitowska, V. Bellani, L. Ortolani, V. Morandi, M. Gazzano, A. Zanelli, S. Borini, V. Palermo, Carbon 84 (2015) 254–262.
[118] H. Wang, K. Sun, F. Tao, D.J. Stacchiola, Y.H. Hu, Angew. Chem. Int. Ed. 52 (2013) 9210–9214.
[119] H. Bi, T. Lin, F. Xu, Y. Tang, Z. Liu, F. Huang, Nano Lett. 16 (2016) 349–354.
[120] T. Lin, I.-W. Chen, F. Liu, C. Yang, H. Bi, F. Xu, F. Huang, Science 350 (2015) 1508–1513.
[121] J. Zhao, W. Ren, H.-M. Cheng, J. Mater. Chem. 22 (2012) 20197–20202.
[122] K.-Y. Shin, J.-Y. Hong, J. Jang, J. Hazard. Mater. 190 (2011) 36–44.
[123] G.L. Zhu, H. Yin, C.Y. Yang, H.L. Cui, Z. Wang, J.J. Xu, T.Q. Lin, F.Q. Huang, Chemcatchem 7 (2015) 2614–2619.
[124] C. Mao, F. Zuo, Y. Hou, X. Bu, P. Feng, Angew. Chem. Int. Ed. 53 (2014) 10485–10489.
[125] H. Tan, Z. Zhao, M. Niu, C. Mao, D. Cao, D. Cheng, P. Feng, Z. Sun, Nanoscale 6 (2014) 10216–10223.
[126] J.J. Xu, Z.L. Tian, G.H. Yin, T.Q. Lin, F.Q. Huang, Dalton Trans. 46 (2017) 1047–1051.
[127] W. Wu, J. Changzhong, V.A.L. Roy, Nanoscale 7 (2015) 38–58.
[128] D. Wang, D. Astruc, Chem. Rev. 114 (2014) 6949–6985.
[129] J. Li, J. Li, Q. Chen, J. Bai, B. Zhou, J. Hazard. Mater. 262 (2013) 304–310.
[130] S. Garcia-Segura, E. Brillas, J. Photochem. Photobiol., C: Photochem. Rev. 31 (2017) 1–35.
[131] M. Zlamal, J.M. Macak, P. Schmuki, J. Krýsa, Electrochem. commun. 9 (2007) 2822–2826.
[132] K. Vinodgopal, S. Hotchandani, P.V. Kamat, J. Phy. Chem. 97 (1993) 9040–9044.
[133] X. Chen, Q. Chen, W. Jiang, Z. Wei, Y. Zhu, Appl. Catal. B: Environ. 211 (2017) 106–113.
[134] Y. Liu, J. Li, B. Zhou, H. Chen, Z. Wang, W. Cai, Chem. Commun. 47 (2011) 10314–10316.
[135] Q. Chen, J. Li, X. Li, K. Huang, B. Zhou, W. Cai, W. Shangguan, Environ. Sci. Technol. 46 (2012) 11451–11458.
[136] L. Xia, J. Bai, J. Li, Q. Zeng, X. Li, B. Zhou, Appl. Catal. B: Environ. 183 (2016) 224–230.
[137] Q. Zeng, L. Lyu, Y. Gao, S. Chang, C. Hu, Appl. Catal. B: Environ. 238 (2018) 309–317.
[138] T. Ochiai, K. Nakata, T. Murakami, A. Fujishima, Y. Yao, D.A. Tryk, Y. Kubota, Water Res. 44 (2010) 904–910.

Wei Zhao obtained his B.E. degree in Material Physics and Chemistry at Wuhan University in China in 2009. He then completed his Ph.D. under the supervision of Prof. Fuqiang Huang at Shanghai Institute of Ceramics, Chinese Academy of Sciences (SICCAS), in 2014. From 2014 to 2016 he worked as a Research Fellow in Prof. Hua Zhang's group at the School of Materials Science and Engineering in Nanyang Technological University in Singapore. He currently holds a position at SICCAS, working on low dimensional nanomaterials for energy conversion and storage.

I-Wei Chen is the Skirkanich Professor of Materials Innovation at the University of Pennsylvania (Penn), with former appointments at the University of Michigan (Materials 1986-1997) and the Massachusetts Institute of Technology (MIT) (Nuclear Engineering; Materials, 1980-1986). He obtained his BS degree in physics in 1972 from Tsinghua University, Taiwan, his MS degree in physics in 1975 from Penn, and his PhD degree in metallurgy in 1980 from MIT. He is an author of more than 100 papers in the *Journal of the American Ceramic Society* on oxide and nitride research, and his 230+ journal papers have been cited more than 13,000 times representing an ISI *h*-index of 63. He holds 16 US patents and conducts current research on thin-film memory devices, energy ceramics and drug delivery. Chen can be reached by email at iweichen@seas.upenn.edu.

Prof. Fuqiang Huang received his Ph.D. in chemistry from Beijing Normal University in 1996. From 1996 to 2003 he worked in the United States as a research staff member in University of Michigan, Northwestern University, Osram Sylvania Inc. and University of Pennsylvania. He became a Professor in Shanghai Institute of Ceramics, Chinese Academy of Sciences in 2004 and joined College of Chemistry and Molecular Engineering, Peking University as a professor in 2010. His current research interests span from energy materials and devices to environmental protection to superconductors.